SIAM J. SCI. COMPUT.
Vol. 40, No. 2, pp. A929–A953

A UNIFORMLY AND OPTIMALLY ACCURATE METHOD FOR THE ZAKHAROV SYSTEM IN THE SUBSONIC LIMIT REGIME*

WEIZHU BAO† AND CHUNMEI SU‡

Abstract. We present two uniformly accurate numerical methods for discretizing the Zakharov system (ZS) with a dimensionless parameter $0 < \varepsilon \leq 1$, which is inversely proportional to the acoustic speed. In the subsonic limit regime, i.e., $0 < \varepsilon \ll 1$, the solution of ZS propagates waves with $O(\varepsilon)$- and $O(1)$-wavelengths in time and space, respectively, and/or rapid outgoing initial layers with speed $O(1/\varepsilon)$ in space due to the singular perturbation of the wave operator in ZS and/or the incompatibility of the initial data. By adopting an asymptotic consistent formulation of ZS, we present a time-splitting exponential wave integrator (TS-EWI) method via applying a time-splitting technique and an exponential wave integrator for temporal derivatives in the nonlinear Schrödinger equation and wave-type equation, respectively. By introducing a multiscale decomposition of ZS, we propose a time-splitting multiscale time integrator (TS-MTI) method. Both methods are explicit and convergent exponentially in space for all kinds of initial data, which is uniformly for $\varepsilon \in (0, 1]$. The TS-EWI method is simpler to be implemented and it is only uniformly and optimally accurate in time for well-prepared initial data, while the TS-MTI method is uniformly and optimally accurate in time for any kind of initial data. Extensive numerical results are reported to show their efficiency and accuracy, especially in the subsonic limit regime. Finally, the TS-MTI method is applied to study numerically convergence rates of ZS to its limiting models when $\varepsilon \to 0^+$.

Key words. Zakharov system, nonlinear Schrödinger equation, subsonic limit regime, exponential wave integrator, asymptotic consistent formulation, multiscale decomposition, time-splitting, multiscale time integrator, uniformly and optimally accurate

AMS subject classifications. 35Q55, 65M06, 65M12, 65M15

DOI. 10.1137/17M1113333

1. Introduction.

We consider the dimensionless Zakharov system (ZS) in d-dimensions ($d = 3, 2, 1$) for describing the propagation of Langmuir waves in plasma [48]

$$
\begin{aligned}
&i\partial_t E(\mathbf{x},t) + \Delta E(\mathbf{x},t) - N(\mathbf{x},t)E(\mathbf{x},t) = 0, \quad \mathbf{x} \in \mathbb{R}^d, \quad t > 0,\\
&\varepsilon^2 \partial_{tt} N(\mathbf{x},t) - \Delta N(\mathbf{x},t) - \Delta |E(\mathbf{x},t)|^2 = 0, \quad \mathbf{x} \in \mathbb{R}^d, \quad t > 0,\\
&E(\mathbf{x},0) = E_0(\mathbf{x}), \quad N(\mathbf{x},0) = N_0^\varepsilon(\mathbf{x}), \quad \partial_t N(\mathbf{x},0) = N_1^\varepsilon(\mathbf{x}), \quad \mathbf{x} \in \mathbb{R}^d,
\end{aligned} \tag{1.1}
$$

where t is time, $\mathbf{x} \in \mathbb{R}^d$ is the spatial coordinate, $E := E(\mathbf{x},t)$ is a complex-valued function representing the varying envelope of a highly oscillatory electric field, $N := N(\mathbf{x},t)$ is a real-valued function representing the fluctuation of the plasma ion density from its equilibrium state, $0 < \varepsilon \leq 1$ is a dimensionless parameter which is inversely proportional to the ion sound speed, and $E_0(\mathbf{x})$, $N_0^\varepsilon(\mathbf{x})$, and $N_1^\varepsilon(\mathbf{x})$ are given functions satisfying $\int_{\mathbb{R}^d} N_1^\varepsilon(\mathbf{x}) d\mathbf{x} = 0$.

*Submitted to the journal's Methods and Algorithms for Scientific Computing section January 24, 2017; accepted for publication (in revised form) January 26, 2018; published electronically March 29, 2018.

http://www.siam.org/journals/sisc/40-2/M111333.html

Funding: The first author's research was supported by Ministry of Education of Singapore grant R-146-000-223-112. The second author's research was supported by Natural Science Foundation of China grant U1530401 and Postdoctoral Science Foundation of China grant 2016M600904.

†Department of Mathematics, National University of Singapore, Singapore 119076 (matbaowz@nus.edu.sg, http://www.math.nus.edu.sg/~bao).

‡Corresponding author. Beijing Computational Science Research Center, Beijing 100193, China, and Department of Mathematics, National University of Singapore, Singapore 119076 (sucm@csrc.ac.cn).

The ZS (1.1) is a classical model for describing mutual interaction between a dispersive wave and a nondispersive (acoustic) wave [18, 30, 40, 42, 48]. It is widely applied in various physical problems, such as in plasma physics (interactions between Langmuir and ion acoustic waves [40, 48]), in hydrodynamics (interactions between short-wave and long-wave gravitational disturbances in the atmosphere [18]), in the theory of molecular chains (interactions of the intramolecular vibrations forming Davydov solitons with the acoustic disturbances in the chain [17]), and so on. In fact, the ZS can be formally derived from the Euler–Maxwell system for a plasma as two interpenetrating fluids—an electron fluid and an ion fluid—under the electromagnetic field by considering a long-wavelength small-amplitude Langmuir oscillation and using asymptotic expansion. For details of the derivation, we refer the reader to [19, 44, 45] and references therein.

It is well known that the ZS (1.1) conserves the *wave energy* [7, 13]

$$\mathcal{M}(t) := \|E(\cdot,t)\|^2 = \int_{\mathbb{R}^d} |E(\mathbf{x},t)|^2 d\mathbf{x} \equiv \int_{\mathbb{R}^d} |E_0(\mathbf{x})|^2 d\mathbf{x} = \mathcal{M}(0), \quad t \geq 0, \tag{1.2}$$

and the *Hamiltonian* [7, 13]

$$\mathcal{L}(t) := \int_{\mathbb{R}^d} \left[|\nabla E|^2 + N|E|^2 + \frac{1}{2}\left(|\nabla U|^2 + |N|^2\right) \right] d\mathbf{x} \equiv \mathcal{L}(0), \quad t \geq 0, \tag{1.3}$$

where $U := U(\mathbf{x},t)$ is defined as

$$-\Delta U(\mathbf{x},t) = \varepsilon \partial_t N(\mathbf{x},t), \quad \mathbf{x} \in \mathbb{R}^d, \quad \lim_{|\mathbf{x}|\to\infty} U(\mathbf{x},t) = 0, \quad t \geq 0. \tag{1.4}$$

For the ZS (1.1) with $\varepsilon = 1$, i.e., $O(1)$-acoustic-speed regime, there are extensive analytical and numerical results in the literature. For the well-posedness in the energy space, we refer the reader to [12, 16, 24, 43] and references therein. In this regime, different efficient and accurate numerical methods have been proposed and analyzed in the literature, such as the finite difference method [14, 15, 26], the time-splitting spectral method [8, 34], the exponential wave integrator (EWI) spectral method [7, 39], the Jacobi-type method [11], the Legendre–Galerkin method [33], the discontinuous-Galerkin method [47], etc. The analytical and numerical results have been extended to the generalized ZS [29, 30, 34] and the vector ZS [7, 34, 44]. However, for the ZS (1.1) with $0 < \varepsilon \ll 1$, i.e., in the subsonic limit regime, the analysis and efficient computation are mathematically and numerically rather complicated issues. The main difficulty is due to that there exist highly oscillatory waves with wavelength at $O(\varepsilon)$ and amplitude at $O(1)$ in time (cf. Figure 1(a)) and/or rapid outgoing initial layers with wave speed at $O(\varepsilon^{-1})$ and amplitude at $O(1)$ in space (cf. Figure 1(b)).

Formally, when $\varepsilon \to 0^+$, $E(\mathbf{x},t) \to E_{\rm s}(\mathbf{x},t)$ and $N(\mathbf{x},t) \to -\rho_{\rm s}(\mathbf{x},t)$ with $\rho_{\rm s}(\mathbf{x},t) := |E_{\rm s}(\mathbf{x},t)|^2$, where $E_{\rm s}(\mathbf{x},t)$ satisfies the nonlinear Schrödinger equation (NLSE) with cubic nonlinearity [35, 38, 41]

$$\begin{aligned} &i\partial_t E_{\rm s}(\mathbf{x},t) + \Delta E_{\rm s}(\mathbf{x},t) + |E_{\rm s}(\mathbf{x},t)|^2 E_{\rm s}(\mathbf{x},t) = 0, \quad \mathbf{x} \in \mathbb{R}^d, \quad t > 0, \\ &E_{\rm s}(\mathbf{x},0) = E_0(\mathbf{x}), \quad \mathbf{x} \in \mathbb{R}^d. \end{aligned} \tag{1.5}$$

Multiplying the first equation in (1.5) by $\overline{E_{\rm s}(\mathbf{x},t)}$ and subtracting from its conjugate, we get

$$\partial_t \rho_{\rm s}(\mathbf{x},t) = -2\,\mathrm{Im}\left(\overline{E_{\rm s}(\mathbf{x},t)}\,\Delta E_{\rm s}(\mathbf{x},t)\right), \quad \mathbf{x} \in \mathbb{R}^d, \quad t \geq 0, \tag{1.6}$$

where $\mathrm{Im}(f)$ and $\overline{f}$ denote the imaginary and complex conjugate parts of f, respectively. Convergence rates of the subsonic limit from the ZS (1.1) to the NLSE (1.5) and initial layers have been analyzed in [35, 38, 41] and references therein. Based on their results, one can decompose the initial data $(N_0^\varepsilon, N_1^\varepsilon)$ in (1.1) as

$$
\begin{aligned}
N_0^\varepsilon(\mathbf{x}) &= -\rho_{\mathrm{s}}(\mathbf{x},0) + \varepsilon^\alpha \omega_0(\mathbf{x}) = -|E_0(\mathbf{x})|^2 + \varepsilon^\alpha \omega_0(\mathbf{x}), \quad \mathbf{x}\in\mathbb{R}^d,\\
N_1^\varepsilon(\mathbf{x}) &= -\partial_t \rho_{\mathrm{s}}(\mathbf{x},0) + \varepsilon^\beta \omega_1(\mathbf{x}) = 2\,\mathrm{Im}\left(\overline{E_0(\mathbf{x})}\,\Delta E_0(\mathbf{x})\right) + \varepsilon^\beta \omega_1(\mathbf{x}),
\end{aligned}
\tag{1.7}
$$

where $\alpha \geq 0$ and $\beta \geq -1$ are parameters describing the incompatibility of the initial data of the ZS (1.1) with respect to that of the NLSE (1.5) in the subsonic limit regime such that the Hamiltonian (1.3) is bounded, and $\omega_0(\mathbf{x})$ and $\omega_1(\mathbf{x})$ are two given real functions independent of ε and satisfying $\int_{\mathbb{R}^d} \omega_1(\mathbf{x})d\mathbf{x} = 0$. Due to the incompatibility of the initial data and/or the singular perturbation of the wave operator, the solution of the ZS (1.1) propagates highly oscillatory waves with wavelength at $O(\varepsilon)$ and $O(1)$ in time and space, respectively, and amplitude at $O(1)$ (cf. Figure 1a), and/or rapid outgoing initial layers with speed at $O(1/\varepsilon)$ and amplitude at $O(1)$ in space (cf. Figure 1b). To illustrate this, Figure 1 displays the solution of (1.1) with (1.7) under $d = 1$, $\alpha = \beta = 0$ and

$$
\begin{aligned}
E_0(x) &= \frac{1}{\sqrt{2}} g\left(\frac{x+18}{10}\right) g\left(\frac{18-x}{9}\right) \sin\left(\frac{x}{2}\right) e^{\frac{\pi}{6}i}, \quad \omega_1(x) = e^{-x^2/3}\sin(2x),\\
\omega_0(x) &= g\left(\frac{x+22}{10}\right) g\left(\frac{22-x}{10}\right) \sin\left(2x+\frac{\pi}{6}\right), \qquad x\in\mathbb{R},
\end{aligned}
\tag{1.8}
$$

with χ_Ω the characteristic function of the domain Ω and

$$
g(x) = \frac{f(x)}{f(x)+f(1-x)}, \qquad f(x) = e^{-1/x}\chi_{(0,\infty)}, \qquad x\in\mathbb{R}.
\tag{1.9}
$$

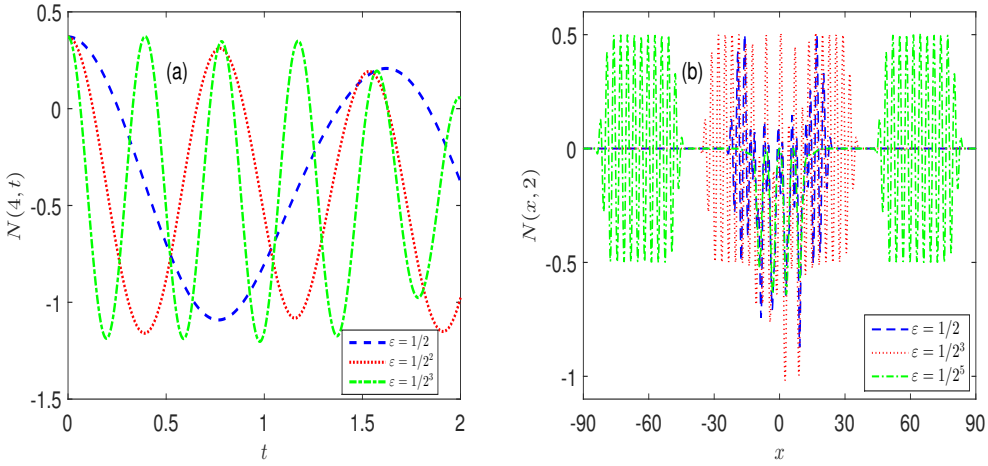

FIG. 1. *Profiles of* $N(x = 4, t)$ (a) *and* $N(x, t = 2)$ (b) *of* (1.1) *with* (1.7), (1.8), *and* (1.9) *under* $d = 1$, $\alpha = \beta = 0$ *for different* ε.

In fact, based on the analysis in [13, 35, 38, 41], when $\alpha \geq 2$ and $\beta \geq 1$, the leading order oscillation is due to the term $\varepsilon^2\partial_{tt}N$ in the ZS, and when either $0 \leq \alpha < 2$ and/or

$-1 \le \beta < 1$, the leading order oscillation is due to the incompatibility of the initial data.

This highly temporal oscillatory nature and/or rapid spatial outgoing initial layers in the solution of the ZS (1.1) make the numerical approximation extremely challenging and costly in the subsonic limit regime, i.e., $0 < \varepsilon \ll 1$. Different numerical methods have been adopted to simulate the dynamics of the ZS in the subsonic limit regime. For example, Bao and Sun [7] presented a Crank–Nicolson leap-frog time-splitting spectral method for solving the ZS, and the numerical experiments suggest that, when ε is small, it requires the meshing strategy $h = O(\varepsilon)$, $\tau = O(\varepsilon)$ with h the mesh size and τ the time step, for initial data with $O(\varepsilon)$ wavelength in space. Recently, by using rigorous numerical analysis, Cai and Yuan [13] established error bounds which depend explicitly on h and τ as well as the small parameter $\varepsilon \in (0, 1]$ of the Crank–Nicolson finite difference (CNFD) method for the ZS (1.1) with initial data at $O(1)$ wavelength in space. Based on their analytical and numerical results, the CNFD method converges at second order in space and 4/3 order in time for $\alpha \ge 2$ and $\beta \ge 1$, which is uniformly for $\varepsilon \in (0, 1]$; and it is *not* uniformly accurate in either space or time when $\alpha = 0$ or $\beta = -1$. Specifically, when $\alpha = 0$ or $\beta = -1$, in order to obtain "correct" physical solution when $0 < \varepsilon \ll 1$, the meshing strategy (or ε-scalability) is required as $h = O(\varepsilon^{1/2})$ and $\tau = O(\varepsilon^{3/2})$. This is a strict and/or strange requirement on the mesh size and time step in the subsonic limit regime since the wavelength in space is at $O(1)$, which is independent of $\varepsilon \in (0, 1]$. Very recently, by introducing an asymptotic consistent formulation of the ZS (1.1), Bao and Su [6] proposed a uniformly accurate finite difference method and established its error bounds (here and afterwards "uniformly" means the error is independent of ε). In space, it is optimally accurate at second order for any initial data ("optimally" means the uniform convergence rate coincides with that of the local truncation error); and in time, it is uniformly accurate at 4/3 order when $\alpha \ge 1$ and $\beta \ge 0$ and, respectively, at $1 + \frac{\min\{\alpha,1+\beta\}}{2+\min\{\alpha,1+\beta\}}$ order when $0 \le \alpha < 1$ and/or $-1 \le \beta < 0$ [6]. Thus the method is uniformly and optimally accurate (UOA) in space. However, it is uniformly accurate while *not* optimally accurate at second order in time for the ZS (1.1) in the subsonic limit regime.

The main aim of this paper is to propose new numerical methods for the ZS (1.1), which are uniformly and optimally accurate in both space and time for $\varepsilon \in (0, 1]$. In the proposed numerical methods, we always adopt the spectral discretization for spatial derivatives. By adopting an asymptotic consistent formulation of ZS [6], we present a time-splitting exponential wave integrator (TS-EWI) method for the ZS (1.1) by applying a time-splitting technique and an EWI for temporal derivatives in the NLSE and wave-type equations, respectively. The method is UOA in both space and time when $\alpha \ge 1$ and $\beta \ge 0$, and it is uniformly accurate in time when $0 \le \alpha < 1$ or $-1 \le \beta < 0$. By introducing a multiscale decomposition of the ZS (1.1), we propose a time-splitting multiscale time integrator (TS-MTI) method which is UOA in both space and time for all kinds of initial data. Another advantage of the TS-MTI method is that the bounded computational domain can be taken as ε-independent, which is very important in high dimensions. Finally, the TS-MTI method is applied to numerically study convergence rates of the ZS (1.1) to its limiting models when $\varepsilon \to 0^+$.

The rest of the paper is organized as follows. In section 2, we recall the asymptotic consistent formulation of the ZS and present the TS-EWI method. In section 3, we introduce a multiscale decomposition of the ZS and propose the TS-MTI method.

Extensive numerical results are reported in section 4 to demonstrate that the proposed methods are uniformly and/or optimally accurate for $\varepsilon \in (0, 1]$. Finally, some concluding remarks are drawn in section 5. Throughout the paper, we adopt the standard Sobolev spaces.

2. A time-splitting exponential wave integrator (TS-EWI) method. In this section, we begin with a review of the asymptotic consistent formulation introduced in [6] for the ZS (1.1) and propose the TS-EWI method by using a time-splitting technique and an EWI for temporal derivatives in the NLSE and wave-type equations, respectively.

2.1. An asymptotic consistent formulation. As introduced in [6], denote $G(\mathbf{x}, t)$ as the solution of the homogeneous wave equation

$$\partial_{tt} G(\mathbf{x}, t) - \frac{1}{\varepsilon^2} \Delta G(\mathbf{x}, t) = 0, \quad \mathbf{x} \in \mathbb{R}^d, \quad t > 0, \tag{2.1}$$

with initial data by noting (1.7)

$$\begin{aligned} &G(\mathbf{x}, 0) = N_0^\varepsilon(\mathbf{x}) + |E_0(\mathbf{x})|^2 = \varepsilon^\alpha \omega_0(\mathbf{x}) := G_0(\mathbf{x}), \quad \mathbf{x} \in \mathbb{R}^d, \\ &\partial_t G(\mathbf{x}, 0) = N_1^\varepsilon(\mathbf{x}) - 2\,\mathrm{Im}(\Delta E_0(\mathbf{x}) \overline{E_0(\mathbf{x})}) = \varepsilon^\beta \omega_1(\mathbf{x}) := G_1(\mathbf{x}), \end{aligned} \tag{2.2}$$

and let

$$F(\mathbf{x}, t) = N(\mathbf{x}, t) + |E(\mathbf{x}, t)|^2 - G(\mathbf{x}, t), \quad \mathbf{x} \in \mathbb{R}^d, \quad t \geq 0. \tag{2.3}$$

Plugging (2.3) into (1.1) and noting (2.1) and (2.2), we obtain an asymptotic consistent formulation (ACF) for the ZS (1.1) [6]

$$\begin{aligned} &i\partial_t E(\mathbf{x}, t) + \Delta E(\mathbf{x}, t) + \left[|E(\mathbf{x}, t)|^2 - F(\mathbf{x}, t) - G(\mathbf{x}, t)\right] E(\mathbf{x}, t) = 0, \\ &\partial_{tt} F(\mathbf{x}, t) - \frac{1}{\varepsilon^2} \Delta F(\mathbf{x}, t) - \partial_{tt} |E(\mathbf{x}, t)|^2 = 0, \quad \mathbf{x} \in \mathbb{R}^d, \quad t > 0, \\ &E(\mathbf{x}, 0) = E_0(\mathbf{x}), \quad F(\mathbf{x}, 0) \equiv 0, \quad \partial_t F(\mathbf{x}, 0) \equiv 0, \quad \mathbf{x} \in \mathbb{R}^d. \end{aligned} \tag{2.4}$$

When $\varepsilon \to 0^+$, formally we have $F(\mathbf{x}, t) \to 0$ and $E(\mathbf{x}, t) \to E_{\mathrm{sop}}(\mathbf{x}, t)$ satisfying the following NLSE with an oscillatory potential (NLSE-OP) [6]

$$\begin{aligned} &i\partial_t E_{\mathrm{sop}}(\mathbf{x}, t) + \Delta E_{\mathrm{sop}}(\mathbf{x}, t) + \left[|E_{\mathrm{sop}}(\mathbf{x}, t)|^2 - G(\mathbf{x}, t)\right] E_{\mathrm{sop}}(\mathbf{x}, t) = 0, \quad t > 0, \\ &E_{\mathrm{sop}}(\mathbf{x}, 0) = E_0(\mathbf{x}), \quad \mathbf{x} \in \mathbb{R}^d. \end{aligned} \tag{2.5}$$

Here we want to emphasize several advantages of the ACF (2.4) over the ZS (1.1) in the subsonic limit regime: (a) the initial data in (1.1) is usually classified into three different categories as (i) well-prepared initial data, i.e., $\alpha \geq 2$ and $\beta \geq 1$, (ii) less ill-prepared initial data, i.e., $1 \leq \alpha < 2$ ($\beta \geq 0$) or $0 \leq \beta < 1$ ($\alpha \geq 0$), and (iii) ill-prepared initial data, i.e., $0 \leq \alpha < 1$ or $-1 \leq \beta < 0$, while the initial data in (2.4) is always well-prepared; (b) although the wavelengths in time for N in (1.1) and F in (2.4) are at $O(\varepsilon)$, however, the amplitudes of N and F are at $O(1)$ and $O(\varepsilon^2)$, respectively (cf. Figures 2 and 3); (c) the highly oscillatory waves and/or rapid outgoing initial layers with amplitude at $O(1)$ due to the incompatibility of the initial data in (1.1) are removed by G in (2.1), which can be solved separately and independently (cf. Figures 2 and 3); and (d) for practical computations, in general, due to fast decay of E at far field and $O(\varepsilon^2)$ in amplitude of F, the bounded computational

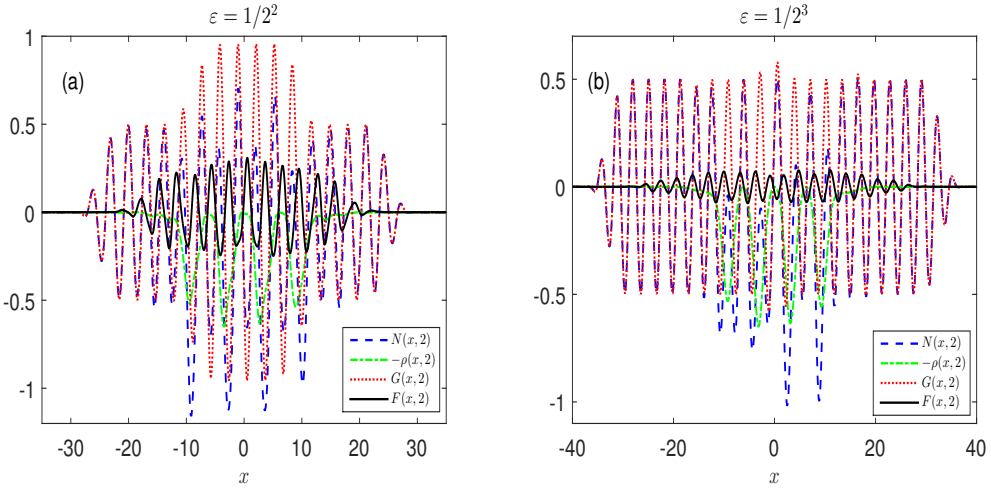

FIG. 2. *Decomposition of* $N(x, t = 2) = -\rho(x, 2) + F(x, 2) + G(x, 2)$ *of* (1.1) *with* (1.7), (1.8), *and* (1.9) *under* $d = 1$, $\alpha = \beta = 0$ *for different* ε.

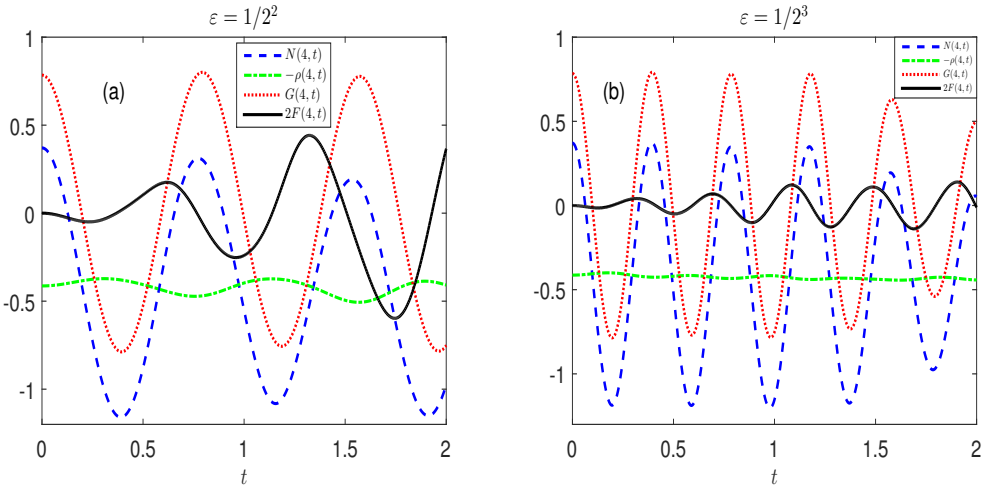

FIG. 3. *Decomposition of* $N(x = 4, t) = -\rho(4, t) + F(4, t) + G(4, t)$ *of* (1.1) *with* (1.7), (1.8), *and* (1.9) *under* $d = 1$, $\alpha = \beta = 0$ *for different* ε.

domain can be chosen much smaller in using the ACF (2.4) compared to that in adopting (1.1) if the simple homogeneous Dirichlet boundary condition is adopted, especially when $0 < \varepsilon \ll 1$.

In order to present the TS-EWI method, for simplicity of notation and without loss of generality, we only present the method in one dimension (1D). Generalizations to higher dimensions are straightforward. Similar to most works for the simulation of the ZS [6, 8, 13, 34], the ACF (2.4) will be truncated into a bounded domain Ω with homogeneous Dirichlet boundary conditions. In general, due to fast decay of the solution at far field, the truncation error can be negligible when Ω is chosen large

enough. In 1D, the ACF (2.4) with $d = 1$ can be approximated by

$$
\begin{aligned}
&i\partial_t E(x,t) + \partial_{xx} E(x,t) + \left[|E(x,t)|^2 - F(x,t) - G(x,t)\right] E(x,t) = 0,\\
&\partial_{tt} F(x,t) - \frac{1}{\varepsilon^2}\partial_{xx} F(x,t) - \partial_{tt}|E(x,t)|^2 = 0, \quad x \in \Omega = (a,b), \quad t > 0,\\
&E(x,0) = E_0(x), \quad F(x,0) \equiv 0, \quad \partial_t F(x,0) \equiv 0, \quad x \in \overline{\Omega},\\
&E(a,t) = E(b,t) = 0, \quad F(a,t) = F(b,t) = 0, \quad t \geq 0.
\end{aligned} \tag{2.6}
$$

2.2. An EWI for the wave-type equation. Let $\tau = \Delta t > 0$ be the time step size, and denote the time steps as $t_k := k\tau$ for $k = 0, 1, 2, \ldots$. Choose a mesh size $h := (b-a)/M$ with M being a positive integer, and denote the grid points as $x_j := a + jh$ for $j = 0, 1, \ldots, M$. Define the index sets

$$
\mathcal{T}_M = \{j \mid j = 1, 2, \ldots, M-1\}, \quad \mathcal{T}_M^0 = \{j \mid j = 0, 1, \ldots, M\},
$$

and denote

$$
X_M := \left\{ v = (v_0, v_1, \ldots, v_M)^T \mid v_0 = v_M = 0 \right\} \subseteq \mathbb{C}^{M+1} \quad \text{with } \|v\|_{l^2}^2 = h \sum_{j=1}^{M-1} |v_j|^2,
$$

$$
Y_M := \operatorname{span}\left\{ \sin(\mu_l (x-a)) \mid l = 1, 2, \ldots, M-1 \right\},
$$

with

$$
\mu_l = \frac{l\pi}{b-a}, \qquad \theta_l = \frac{\mu_l}{\varepsilon} = O\left(\frac{1}{\varepsilon}\right), \qquad l \in \mathcal{T}_M. \tag{2.7}
$$

For any function $\psi(x) \in H_0^1(\Omega)$ and $\phi(x) \in C_0(\overline{\Omega})$ and vector $\phi = (\phi_0, \phi_1, \ldots, \phi_M)^T \in X_M$, let $\mathcal{P}_M : H_0^1(\Omega) \to Y_M$ be the standard L^2-projection operator, and let $I_M : C_0(\overline{\Omega}) \to Y_M$ or $I_M : X_M \to Y_M$ be the standard interpolation operator as

$$
(\mathcal{P}_M \psi)(x) = \sum_{l=1}^{M-1} \widehat{\psi}_l \sin\left(\mu_l (x-a)\right), \quad (I_M \phi)(x) = \sum_{l=1}^{M-1} \widetilde{\phi}_l \sin\left(\mu_l (x-a)\right), \tag{2.8}
$$

where $\widehat{\psi}_l$ and $\widetilde{\phi}_l$ are the sine and discrete sine transform coefficients of the function $\psi(x)$ and vector ϕ (with $\phi_j = \phi(x_j)$ for $j \in \mathcal{T}_M^0$ when involved), respectively, defined as

$$
\widehat{\psi}_l = \frac{2}{b-a} \int_a^b \psi(x) \sin(\mu_l (x-a)) dx, \quad \widetilde{\phi}_l = \frac{2}{M} \sum_{j=1}^{M-1} \phi_j \sin\left(\frac{jl\pi}{M}\right), \quad l \in \mathcal{T}_M. \tag{2.9}
$$

For the wave-type equation in (2.6), we discretize it in space by the sine spectral method and in time by an EWI which has been widely used for discretizing second-order ODEs [27, 28] and oscillatory PDEs [2, 3, 32]. Specifically, find $F_M := F_M(x,t)$, i.e.,

$$
F_M(x,t) = \sum_{l=1}^{M-1} \widehat{F}_l(t) \sin(\mu_l (x-a)), \tag{2.10}
$$

such that

$$
\partial_{tt} F_M - \frac{1}{\varepsilon^2}\partial_{xx} F_M = \mathcal{P}_M(\partial_{tt}\rho) \quad \text{with} \quad \rho := \rho(x,t) = |E(x,t)|^2. \tag{2.11}
$$

Substituting (2.10) into (2.11) and noticing the orthogonality of $\sin(\mu_l(x-a))$ for $l \in \mathcal{T}_M$, we obtain with $t = t_k + s$ for $k \geq 0$ and $s \in \mathbb{R}$

$$\frac{d^2}{ds^2}\widehat{F}_l(t_k+s) + \theta_l^2 \widehat{F}_l(t_k+s) - \frac{d^2}{ds^2}\widehat{(\rho^k)}_l(s) = 0, \qquad l \in \mathcal{T}_M, \tag{2.12}$$

where

$$\begin{aligned} &\rho^k(x,s) := \rho(x, t_k+s), \qquad \widehat{(\rho^k)}_l(s) = \widehat{\rho}_l(t_k+s), \\ &\widehat{(\rho^k)}_l'(s) = \widehat{(\partial_s \rho)}_l(t_k+s), \quad \widehat{(\rho^k)}_l''(s) = \widehat{(\partial_{ss}\rho)}_l(t_k+s). \end{aligned} \tag{2.13}$$

The variation-of-constant formula for (2.12) gives [27, 28]

$$\widehat{F}_l(t_k+s) = \cos(\theta_l s)\widehat{F}_l(t_k) + \frac{\sin(\theta_l s)}{\theta_l}\widehat{F}_l'(t_k) + \frac{1}{\theta_l}\int_0^s \widehat{(\rho^k)}_l''(\omega)\sin\left(\theta_l(s-\omega)\right)d\omega. \tag{2.14}$$

Differentiating (2.14) with respect to s, we obtain

$$\widehat{F}_l'(t_k+s) = -\theta_l \sin(\theta_l s)\widehat{F}_l(t_k) + \cos(\theta_l s)\widehat{F}_l'(t_k) + \int_0^s \widehat{(\rho^k)}_l''(\omega)\cos\left(\theta_l(s-\omega)\right)d\omega. \tag{2.15}$$

For $k = 0$, setting $s = \tau$ in (2.14) and (2.15) and using the initial condition in (2.4), integrating by parts, and approximating integrals via the Gautschi-type quadrature [3, 23, 31], we get

$$\begin{aligned} \widehat{F}_l(t_1) &= \cos(\tau\theta_l)\widehat{F}_l(0) + \frac{\sin(\tau\theta_l)}{\theta_l}\widehat{F}_l'(0) + \frac{1}{\theta_l}\int_0^\tau \widehat{(\rho^0)}_l''(\omega)\sin\left(\theta_l(\tau-\omega)\right)d\omega \\ &= \frac{1}{\theta_l}\int_0^\tau \widehat{(\rho^0)}_l''(\omega)\sin\left(\theta_l(\tau-\omega)\right)d\omega \\ &= -\frac{\sin(\tau\theta_l)}{\theta_l}\widehat{(\rho^0)}_l'(0) + \int_0^\tau \widehat{(\rho^0)}_l'(\omega)\cos\left(\theta_l(\tau-\omega)\right)d\omega \\ &\approx -\frac{\sin(\tau\theta_l)}{\theta_l}\widehat{(\rho^0)}_l'(0) + \int_0^\tau \left[\widehat{(\rho^0)}_l'(0) + w\,\widehat{(\rho^0)}_l''(0)\right]\cos\left(\theta_l(\tau-\omega)\right)d\omega \\ &= -\frac{\sin(\tau\theta_l)}{\theta_l}\widehat{(\rho^0)}_l'(0) + \frac{\sin(\tau\theta_l)}{\theta_l}\widehat{(\rho^0)}_l'(0) + d_l\,\widehat{(\rho^0)}_l''(0) \\ &= d_l\,\widehat{(\rho^0)}_l''(0), \qquad l \in \mathcal{T}_M; \end{aligned} \tag{2.16}$$

$$\begin{aligned} \widehat{(F)}_l'(t_1) &= \int_0^\tau \widehat{(\rho^0)}_l''(\omega)\cos\left(\theta_l(\tau-\omega)\right)d\omega \\ &= \widehat{(\rho^0)}_l'(\tau) - \cos(\tau\theta_l)\widehat{(\rho^0)}_l'(0) - \theta_l\int_0^\tau \widehat{(\rho^0)}_l'(\omega)\sin(\theta_l(\tau-\omega))d\omega \\ &\approx \widehat{(\rho^0)}_l'(\tau) - \cos(\tau\theta_l)\widehat{(\rho^0)}_l'(0) - \theta_l\int_0^\tau \left[\widehat{(\rho^0)}_l'(0) + w\,\widehat{(\rho^0)}_l''(0)\right]\sin(\theta_l(\tau-\omega))d\omega \\ &= \widehat{(\rho^1)}_l'(0) - \cos(\tau\theta_l)\widehat{(\rho^0)}_l'(0) - [1-\cos(\tau\theta_l)]\widehat{(\rho^0)}_l'(0) - b_l\,\theta_l\,\widehat{(\rho^0)}_l''(0) \\ &= \widehat{(\rho^1)}_l'(0) - \widehat{(\rho^0)}_l'(0) - b_l\,\theta_l\,\widehat{(\rho^0)}_l''(0), \end{aligned} \tag{2.17}$$

where

$$
\begin{aligned}
a_l &= \int_0^\tau \sin(\theta_l(\tau-\omega))d\omega = \frac{1-\cos(\tau\theta_l)}{\theta_l} = O(\varepsilon),\\
b_l &= \int_0^\tau \omega\sin(\theta_l(\tau-\omega))d\omega = \frac{\tau\theta_l-\sin(\tau\theta_l)}{\theta_l^2} = O(\varepsilon),\\
c_l &= \int_0^\tau \cos(\theta_l(\tau-\omega))d\omega = \frac{\sin(\tau\theta_l)}{\theta_l} = O(\varepsilon),\\
d_l &= \int_0^\tau \omega\cos(\theta_l(\tau-\omega))d\omega = \frac{1-\cos(\tau\theta_l)}{\theta_l^2} = O(\varepsilon^2), \qquad l\in\mathcal{T}_M.
\end{aligned}
$$

For $k\geq 1$, summing (2.14) with $s=\tau$ and $s=-\tau$ together, and approximating integrals via the Gautschi-type quadrature [3, 23, 31], we obtain

$$
\begin{aligned}
\widehat{F}_l(t_{k+1}) &= 2\cos(\tau\theta_l)\widehat{F}_l(t_k) - \widehat{F}_l(t_{k-1}) + \frac{1}{\theta_l}\int_0^\tau \widehat{(\rho_+^k)}_l''(\omega)\sin(\theta_l(\tau-\omega))d\omega\\
&\approx 2\cos(\tau\theta_l)\widehat{F}_l(t_k) - \widehat{F}_l(t_{k-1}) + \frac{1}{\theta_l}\int_0^\tau \widehat{(\rho_+^k)}_l''(0)\sin(\theta_l(\tau-\omega))d\omega\\
&= 2\cos(\tau\theta_l)\widehat{F}_l(t_k) - \widehat{F}_l(t_{k-1}) + 2\frac{a_l}{\theta_l}\widehat{(\rho^k)}_l''(0)\\
&= 2\cos(\tau\theta_l)\widehat{F}_l(t_k) - \widehat{F}_l(t_{k-1}) + 2d_l\widehat{(\rho^k)}_l''(0), \qquad (2.18)
\end{aligned}
$$

where $\widehat{(\rho_+^k)}_l''(\omega) = \widehat{(\rho^k)}_l''(\omega) + \widehat{(\rho^k)}_l''(-\omega)$ is an even function satisfying $\widehat{(\rho_+^k)}_l'''(0)=0$. Carrying out a similar procedure to (2.15) with subtraction instead of summation, we get

$$
\begin{aligned}
\widehat{F}_l'(t_{k+1}) &= \widehat{F}_l'(t_{k-1}) - 2\theta_l\sin(\tau\theta_l)\widehat{F}_l(t_k) + \int_0^\tau \widehat{(\rho_+^k)}_l''(\omega)\cos(\theta_l(\tau-\omega))d\omega\\
&\approx \widehat{F}_l'(t_{k-1}) - 2\theta_l\sin(\tau\theta_l)\widehat{F}_l(t_k) + \int_0^\tau \widehat{(\rho_+^k)}_l''(0)\cos(\theta_l(\tau-\omega))d\omega\\
&= \widehat{F}_l'(t_{k-1}) - 2\theta_l\sin(\tau\theta_l)\widehat{F}_l(t_k) + 2c_l\widehat{(\rho^k)}_l''(0). \qquad (2.19)
\end{aligned}
$$

Multiplying the first equation in (2.6) by $\overline{E(x,t)}$ and subtracting from its conjugate, we get

$$
\partial_t\rho(x,t) = -2\,\mathrm{Im}\left(\overline{E(x,t)}\,\partial_{xx}E(x,t)\right), \qquad \mathbf{x}\in\mathbb{R}, \quad t\geq 0. \tag{2.20}
$$

Differentiating (2.20) with respect to t, we obtain

$$
\partial_{tt}\rho(x,t) = -2\,\mathrm{Im}\left(\overline{\partial_t E(x,t)}\,\partial_{xx}E(x,t) + \overline{E(x,t)}\,\partial_{xxt}E(x,t)\right). \tag{2.21}
$$

Taking $t=t_k$ in (2.20) and (2.21), noting (2.13) with $s=0$, we have

$$
\begin{aligned}
\partial_t\rho(x,t_k) &= -2\,\mathrm{Im}\left(\overline{E(x,t_k)}\,\partial_{xx}E(x,t_k)\right),\\
\partial_{tt}\rho(x,t_k) &= -2\,\mathrm{Im}\left(\overline{\partial_t E(x,t_k)}\,\partial_{xx}E(x,t_k) + \overline{E(x,t_k)}\,\partial_{xxt}E(x,t_k)\right),
\end{aligned} \tag{2.22}
$$

where

$$
\partial_t E(x,t_k) = i\left[\partial_{xx}E(x,t_k) + E(x,t_k)\left(|E(x,t_k)|^2 - F(x,t_k) - G(x,t_k)\right)\right].
$$

Then $\widehat{(\rho^k)}_l'(0)$ and $\widehat{(\rho^k)}_l''(0)$ $(l\in\mathcal{T}_M)$ are the sine transform coefficients of $\partial_t\rho(x,t_k)$ and $\partial_{tt}\rho(x,t_k)$, respectively, for $k\geq 0$.

2.3. A time-splitting method for NLSE. For the NLSE in (2.6), we adopt the time-splitting sine pseudospectral (TSSP) method, which has been widely used in the literature [4, 5, 8, 10, 34, 36, 46]. From time $t = t_k$ to $t = t_{k+1}$ by writing $t = t_k + s$, the NLSE in (2.6) is solved in three splitting steps. One solves first

$$i\partial_s E(x, t_k + s) + \partial_{xx} E(x, t_k + s) = 0, \quad s \geq 0, \tag{2.23}$$

for a half time step of length $\tau/2$, followed by solving the equation

$$i\partial_s E(x, t_k + s) = \left[-|E(x, t_k + s)|^2 + F(x, t_k + s) + G(x, t_k + s)\right] E(x, t_k + s) \tag{2.24}$$

for time step τ, and followed by integrating (2.23) for another $\tau/2$.

For the free Schrödinger equation (2.23) with a homogeneous Dirichlet boundary condition, one can discretize it in space by the sine spectral method and then integrate the ODEs *exactly* in phase space (or Fourier space). Multiplying (2.24) by $\overline{E(x, t_k + s)}$ and then summing it with its complex conjugate [8, 34], one can deduce that $\partial_s |E(x, t_k + s)|^2 = 0$ for $s \geq 0$, which suggests that $|E(x, t_k + s)| \equiv |E(x, t_k)|$ for $s \geq 0$ and $x \in \overline{\Omega}$ and (2.24) is indeed a linear ODE for each fixed $x \in \overline{\Omega}$. Thus we can integrate (2.24) *analytically* and obtain

$$\begin{aligned} E(x, t_k + \tau) &= E(x, t_k) e^{i \int_0^\tau \left[|E(x,t_k)|^2 - F(x,t_k+s) - G(x,t_k+s)\right] ds} \\ &= E(x, t_k) e^{i\tau[|E(x,t_k)|^2 - F^{k+1/2}(x) - G^{k+1/2}(x)]}, \end{aligned} \tag{2.25}$$

where

$$F^{k+1/2}(x) = \frac{1}{\tau} \int_0^\tau F(x, t_k + s) ds \approx \frac{1}{2}(F(x, t_k) + F(x, t_{k+1})), \tag{2.26}$$

$$G^{k+1/2}(x) = \frac{1}{\tau} \int_0^\tau G(x, t_k + s) ds, \qquad x \in \overline{\Omega}. \tag{2.27}$$

2.4. The TS-EWI method. Combining the TSSP method for the NLSE and EWI for the wave-type equation in (2.6), we immediately obtain the TS-EWI method. In practical computation, the integrals for computing the sine transform coefficients in (2.16)–(2.19) are usually approximated by numerical quadratures on the grid points. Let E_j^k, F_j^k, and $\dot{F}_j^k$ be the approximations of $E(x_j, t_k)$, $F(x_j, t_k)$, and $\partial_t F(x_j, t_k)$, respectively, and denote $\rho_j^k = |E_j^k|^2$, $\dot{\rho}_j^k$, and $\ddot{\rho}_j^k$ as the approximations of $\rho(x_j, t_k)$, $\partial_t \rho(x_j, t_k)$, and $\partial_{tt} \rho(x_j, t_k)$, respectively, for $j \in \mathcal{T}_M^0$ and $k \geq 0$. Choosing $E_j^0 = E_0(x_j)$, $F_j^0 = \dot{F}_j^0 = 0$ for $j \in \mathcal{T}_M^0$, the TS-EWI method for computing E_j^{k+1} and F_j^{k+1} reads as

$$\begin{aligned} F_j^{k+1} &= \sum_{l=1}^{M-1} \widetilde{(F^{k+1})}_l \sin\left(\frac{jl\pi}{M}\right), \\ E_j^{(1)} &= \sum_{l=1}^{M-1} e^{-i\tau\mu_l^2/2} \widetilde{(E^k)}_l \sin\left(\frac{jl\pi}{M}\right), \qquad j \in \mathcal{T}_M^0, \\ E_j^{(2)} &= E_j^{(1)} e^{i\tau\left[|E_j^{(1)}|^2 - (F_j^k + F_j^{k+1})/2 - G_j^{k+\frac{1}{2}}\right]}, \\ E_j^{k+1} &= \sum_{l=1}^{M-1} e^{-i\tau\mu_l^2/2} \widetilde{(E^{(2)})}_l \sin\left(\frac{jl\pi}{M}\right), \end{aligned} \tag{2.28}$$

where

$$(\widetilde{F^{k+1}})_l = \begin{cases} d_l(\widetilde{\ddot{\rho}^0})_l, & k=0, \\ 2\cos(\tau\theta_l)(\widetilde{F^k})_l - (\widetilde{F^{k-1}})_l + 2d_l(\widetilde{\ddot{\rho}^k})_l, & k \geq 1, \end{cases} \tag{2.29}$$
$$G_j^{k+\frac{1}{2}} = \frac{1}{\tau}\int_0^\tau G(x_j, t_k+s)ds, \quad \ddot{\rho}_j^k = -2\,\mathrm{Im}\left[\overline{\dot{E}_j^k}\, D_{xx}E_j^k + \overline{E_j^k}\, D_{xx}\dot{E}_j^k\right],$$

with

$$\dot{E}_j^k = i\left[D_{xx}E_j^k + (|E_j^k|^2 - F_j^k - G_j^k)E_j^k\right], \quad G_j^k = G(x_j,t_k), \quad j \in \mathcal{T}_M^0, \quad k \geq 0.$$

Here $G(x,t)$ is the solution of the wave equation (2.1) with initial data (2.2) and D_{xx} is the sine pseudospectral approximation to ∂_{xx}, which is defined as [1]

$$D_{xx}\psi_j = -\sum_{l=1}^{M-1} \frac{\sin(\mu_l^2\tau)}{\tau}\widetilde{(\psi)}_l \sin\left(\frac{jl\pi}{M}\right), \quad j \in \mathcal{T}_M^0. \tag{2.30}$$

Finally, let N_j^k and $\dot{N}_j^k$ be the approximations of $N(x_j,t_k)$ and $\partial_t N(x_j,t_k)$, respectively, and take $N_j^0 = N_0^\varepsilon(x_j)$ and $\dot{N}_j^0 = N_1^\varepsilon(x_j)$ for $j \in \mathcal{T}_M^0$. Noting (2.3), we have for $k \geq 0$,

$$N_j^{k+1} = -|E_j^{k+1}|^2 + F_j^{k+1} + G_j^{k+1}, \ \dot{N}_j^{k+1} = -\dot{\rho}_j^{k+1} + \dot{F}_j^{k+1} + \dot{G}_j^{k+1}, \ j \in \mathcal{T}_M^0, \tag{2.31}$$

where

$$\dot{G}_j^{k+1} = \partial_t G(x_j, t_{k+1}), \quad \dot{F}_j^{k+1} = \sum_{l=1}^{M-1} (\widetilde{\dot{F}^{k+1}})_l \sin\left(\frac{jl\pi}{M}\right),$$

with

$$(\widetilde{\dot{F}^{k+1}})_l = \begin{cases} (\widetilde{\dot{\rho}^1})_l - (\widetilde{\dot{\rho}^0})_l - b_l\theta_l(\widetilde{\ddot{\rho}^0})_l, & k=0, \\ (\widetilde{\dot{F}^{k-1}})_l - 2\theta_l\sin(\tau\theta_l)(\widetilde{F^k})_l + 2c_l(\widetilde{\ddot{\rho}^k})_l, & k \geq 1, \end{cases}$$
$$\dot{\rho}_j^k = -2\,\mathrm{Im}\left(\overline{E_j^k}D_{xx}E_j^k\right), \quad j \in \mathcal{T}_M^0, \quad k \geq 0.$$

The TS-EWI method (2.28) for the ZS (2.6) is explicit, time symmetric, easy to be implemented, and very efficient due to the fast discrete sine transform (DST). The memory cost is $O(M)$, and the computational cost per time step is $O(M\log M)$. Moreover, it conserves the wave energy (1.2) in the discretized level, i.e.,

$$\|E^k\|_{l^2}^2 := h\sum_{j=1}^{M-1}|E_j^k|^2 \equiv \|E^0\|_{l^2}^2 = h\sum_{j=1}^{M-1}|E_0(x_j)|^2, \qquad k \geq 0. \tag{2.32}$$

We remark here that for the linear wave equation (2.1), one can either get its analytical solution by the d'Alembert formula [21] or find its numerical solution on a bounded computational domain with a proper boundary condition via the method of line discretization in space and then integrate in time analytically to get G_j^k, $\dot{G}_j^k$, and $G_j^{k+\frac{1}{2}}$ for $k \geq 0$ and $j \in \mathcal{T}_M^0$ [6]. If one solves it numerically on a bounded computational domain with the simple homogeneous Dirichlet boundary condition, then the bounded computational domain Ω_ε has to be chosen as ε-dependent due to the fact that the rapid outgoing waves are at wave speed $O\left(\frac{1}{\varepsilon}\right)$ and at amplitude

$O(1)$ to avoid the truncation error. Of course, if one adapts the accurate and/or high order perfect matched layer (PML) [9] or the transparent boundary condition (TBC) [22, 25] or the absorbing boundary condition (ABC) [20] for the linear wave equation (2.1) during the truncation, then one can choose the bounded computational domain as ε-independent, which can be significantly smaller compared to Ω_ε in the subsonic limit regime, i.e., $0 < \varepsilon \ll 1$.

3. A time-splitting multiscale time integrator (TS-MTI) method. In this section, we introduce a multiscale decomposition of the ZS (1.1) and present the TS-MTI method by applying a time-splitting technique and a multiscale time integrator for temporal derivatives in the NLSE and wave-type equations, respectively.

3.1. A multiscale decomposition. Let $\tau = \Delta t > 0$ be the time step size, and denote the time steps as $t_k := k\tau$ for $k = 0, 1, 2, \ldots$. Here we present a multiscale decomposition for the solution of the ZS (1.1) on the time interval $[t_k, t_{k+1}]$ with given initial data at $t = t_k$ as

$$E_0^k(\mathbf{x}) := E(\mathbf{x}, t_k), \quad N_0^k(\mathbf{x}) := N(\mathbf{x}, t_k), \quad N_1^k(\mathbf{x}) := \partial_t N(\mathbf{x}, t_k), \qquad \mathbf{x} \in \mathbb{R}^d. \tag{3.1}$$

Similar to the introduction of the ACF for the ZS (1.1), for $k \geq 0$, we introduce $F^k(\mathbf{x}, s) \in \mathbb{R}$ as

$$F^k(\mathbf{x}, s) = N(\mathbf{x}, t_k + s) + |E(\mathbf{x}, t_k + s)|^2 - G^k(\mathbf{x}, s), \quad \mathbf{x} \in \mathbb{R}^d, \quad 0 \leq s \leq \tau, \tag{3.2}$$

where $G^k(\mathbf{x}, s) \in \mathbb{R}$ is the solution of the homogeneous wave equation

$$\partial_{ss} G^k(\mathbf{x}, s) - \frac{1}{\varepsilon^2} \Delta G^k(\mathbf{x}, s) = 0, \quad \mathbf{x} \in \mathbb{R}^d, \quad 0 \leq s \leq \tau, \tag{3.3}$$

with initial data by noting (3.1)

$$\begin{aligned} &G^k(\mathbf{x}, 0) = N_0^k(\mathbf{x}) + |E_0^k(\mathbf{x})|^2 := G_0^k(\mathbf{x}), \quad \mathbf{x} \in \mathbb{R}^d, \\ &\partial_s G^k(\mathbf{x}, 0) = N_1^k(\mathbf{x}) - 2\,\mathrm{Im}\left(\overline{E_0^k(\mathbf{x})} \Delta E_0^k(\mathbf{x})\right) := G_1^k(\mathbf{x}). \end{aligned} \tag{3.4}$$

Plugging (3.2) into (1.1) and noting (3.3) and (3.4), we obtain a multiscale decomposition formulation (MDF) for the ZS (1.1) with $E^k(\mathbf{x}, s) := E(\mathbf{x}, t_k + s)$ for $s \in [0, \tau]$ as

$$\begin{aligned} &i\partial_s E^k(\mathbf{x}, s) + \Delta E^k(\mathbf{x}, s) + \left[|E^k(\mathbf{x}, s)|^2 - F^k(\mathbf{x}, s) - G^k(\mathbf{x}, s)\right] E^k(\mathbf{x}, s) = 0, \\ &\partial_{ss} F^k(\mathbf{x}, s) - \frac{1}{\varepsilon^2} \Delta F^k(\mathbf{x}, s) - \partial_{ss} |E^k(\mathbf{x}, s)|^2 = 0, \quad \mathbf{x} \in \mathbb{R}^d, \quad s \in [0, \tau], \\ &E^k(\mathbf{x}, 0) = E_0^k(\mathbf{x}), \quad F^k(\mathbf{x}, 0) \equiv 0, \quad \partial_s F^k(\mathbf{x}, 0) \equiv 0, \quad \mathbf{x} \in \mathbb{R}^d. \end{aligned} \tag{3.5}$$

After solving the decomposed system (3.5), we can get immediately $E_0^{k+1}(\mathbf{x}) := E^k(\mathbf{x}, \tau) = E(\mathbf{x}, t_{k+1}) = E^{k+1}(\mathbf{x}, 0)$, $F^k(\mathbf{x}, \tau)$, and $\partial_s F^k(\mathbf{x}, \tau)$. Then we can reconstruct $N_0^{k+1}(\mathbf{x}) := N(\mathbf{x}, t_{k+1})$ and $N_1^{k+1}(\mathbf{x}) := \partial_t N(\mathbf{x}, t_{k+1})$ via (3.2) as

$$\begin{aligned} N(\mathbf{x}, t_{k+1}) &= -|E_0^{k+1}(\mathbf{x})|^2 + F^k(\mathbf{x}, \tau) + G^k(\mathbf{x}, \tau), \qquad \mathbf{x} \in \mathbb{R}^d, \\ \partial_t N(\mathbf{x}, t_{k+1}) &= -\partial_s |E^k|^2(\mathbf{x}, \tau) + \partial_s F^k(\mathbf{x}, \tau) + \partial_s G^k(\mathbf{x}, \tau) \\ &= 2\,\mathrm{Im}(\overline{E_0^{k+1}(\mathbf{x})} \Delta E_0^{k+1}(\mathbf{x})) + \partial_s F^k(\mathbf{x}, \tau) + \partial_s G^k(\mathbf{x}, \tau), \end{aligned} \tag{3.6}$$

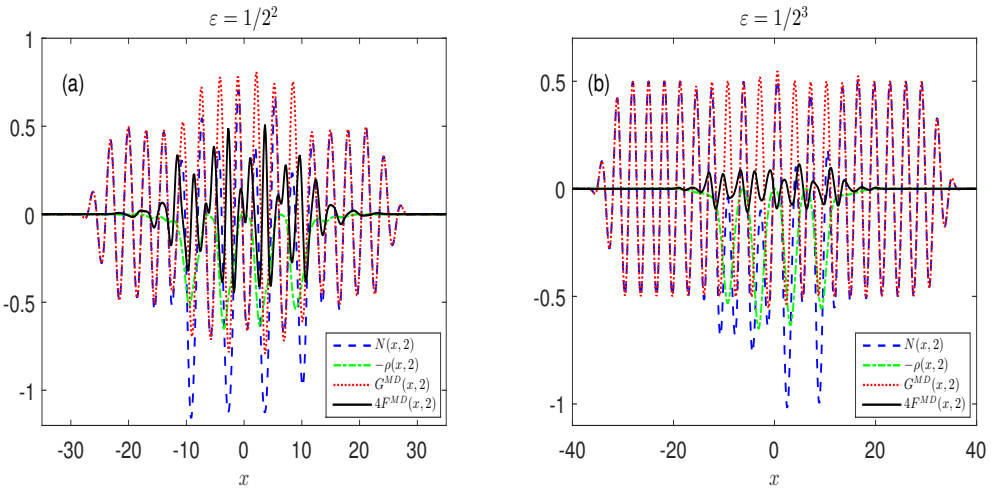

FIG. 4. *Decomposition of* $N(x,t=2) = -\rho(x,2) + F^{MD}(x,2) + G^{MD}(x,2)$ *of* (1.1) *with* (1.7), (1.8), *and* (1.9) *under* $d=1$, $\alpha=\beta=0$ *via the MDF* (3.2)–(3.6) *with* $\tau = 0.5$ *for different* ε.

which immediately implies that

$$
\begin{aligned}
&G_0^{k+1}(\mathbf{x}) = N_0^{k+1}(\mathbf{x}) + |E_0^{k+1}(\mathbf{x})|^2 = F^k(\mathbf{x},\tau) + G^k(\mathbf{x},\tau), \qquad \mathbf{x}\in\mathbb{R}^d,\\
&G_1^{k+1}(\mathbf{x}) = N_1^{k+1}(\mathbf{x}) - 2\,\mathrm{Im}\left(\overline{E_0^{k+1}(\mathbf{x})}\Delta E_0^{k+1}(\mathbf{x})\right) = \partial_s F^k(\mathbf{x},\tau) + \partial_s G^k(\mathbf{x},\tau).
\end{aligned} \tag{3.7}
$$

We remark here that $F^k(\mathbf{x},\tau) \neq F^{k+1}(\mathbf{x},0)$ and $G^k(\mathbf{x},\tau) \neq G^{k+1}(\mathbf{x},0)$. Define

$$
G^{MD}(\mathbf{x},t_k+s) = G^k(\mathbf{x},s),\ F^{MD}(\mathbf{x},t_k+s) = F^k(\mathbf{x},s),\ 0\le s<\tau,\ k\ge 0; \tag{3.8}
$$

then we know $G^{MD}(\mathbf{x},t)$ satisfies the homogeneous wave equation (3.3) over each interval $[t_k,t_{k+1})$ for $k\ge 0$ and

$$
F^{MD}(\mathbf{x},t_k)\equiv 0, \quad \partial_t F^{MD}(\mathbf{x},t_k)\equiv 0, \quad \mathbf{x}\in\mathbb{R}^d.
$$

Of course, $G^{MD}(\mathbf{x},t)$ and $F^{MD}(\mathbf{x},t)$ have jumps at $t=t_k$ for $k\ge 1$.

Here we want to emphasize several advantages of the MDF (3.2)–(3.6) over the ACF (2.4) in the subsonic limit regime: (a) the initial data for F^k in (3.5) is always zero for all $k\ge 0$, while $F(\mathbf{x},t_k)$ in (2.4) is nonzero when $k\ge 1$; (b) the amplitude of F^k in (3.5) (and thus $F^{MD}(\mathbf{x},t)$) is at $O(\min\{\varepsilon^2,\tau^2\})$ for $k\ge 0$, while the amplitude of F in (2.4) is at $O(\varepsilon^2)$ (cf. Figures 4 and 5); (c) due to the homogeneous initial condition of F^k, the essential support of F^{MD} in the MDF (3.2)–(3.6) is $[-C-\frac{\tau}{\varepsilon}, C+\frac{\tau}{\varepsilon}]$ ($[-C,C]$ is the essential support of E, which is independent of ε because of its convergence to the solution of the Schrödinger equation (1.5) [38]), which implies that the support of F^{MD} can be essentially independent of $0<\varepsilon\le 1$ when $\tau\lesssim\varepsilon$ subject to truncation error depending on $O(\tau^2)$, while that of F in (2.4) is still at $[-C-\frac{t}{\varepsilon}, C+\frac{t}{\varepsilon}]$ (cf. Figures 2 and 4); and (d) for practical computations, in general, due to fast decay of E at far field, and essentially bounded support of F^k when $\tau\lesssim\varepsilon$ and at $O(\min\{\varepsilon^2,\tau^2\})$ in amplitude of F^k, the bounded computational domain can be chosen independent of $0<\varepsilon\le 1$ in using the MDF (3.2)–(3.6) compared to that in adopting the ACF (2.4), especially in the regime $\tau=O(\varepsilon)$ and $0<\varepsilon\ll 1$.

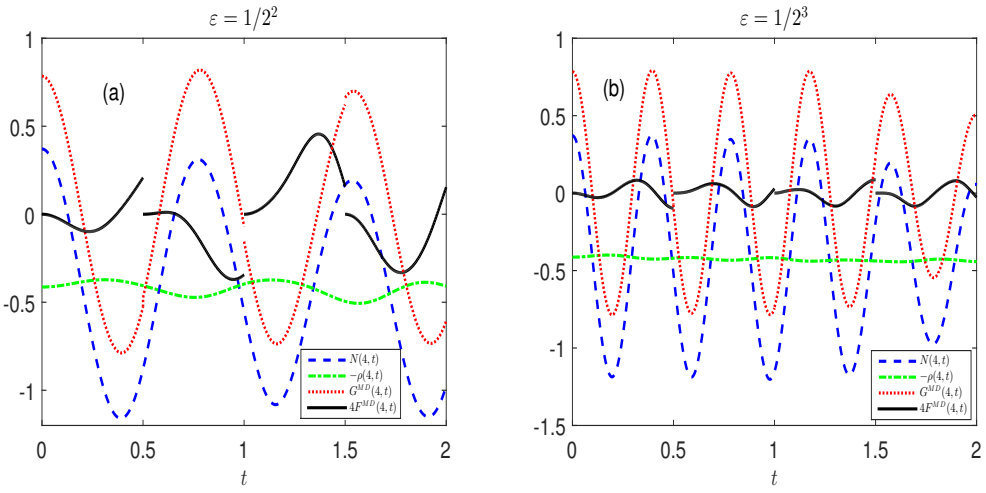

FIG. 5. *Decomposition of* $N(x=4,t) = -\rho(4,t) + F^{MD}(4,t) + G^{MD}(4,t)$ *of* (1.1) *with* (1.7), (1.8), *and* (1.9) *under* $d=1$, $\alpha=\beta=0$ *via the MDF* (3.2)–(3.6) *with* $\tau = 0.5$ *for different* ε.

3.2. The TS-MTI method. Similar to section 2 for discretizing the ACF (2.4), the MDF (3.5) can be discretized in a similar way. Specifically, we can truncate (3.5) in 1D on a bounded interval $\Omega = (a,b)$ with a homogeneous Dirichlet boundary condition. Then the NLSE in (3.5) can be discretized by the TSSP method with details omitted here for brevity. The wave-type equation in (3.5) will be discretized in space by the sine spectral method and in time by the EWI method, i.e., find

$$F_M^k(x,s) = \sum_{l=1}^{M-1} \widehat{(F^k)}_l(s) \sin(\mu_l(x-a)), \quad a \le x \le b, \quad 0 \le s \le \tau. \tag{3.9}$$

Plugging (3.9) into (3.5), noticing the initial condition, and using the variation-of-constant formula, we get

$$\begin{aligned} \widehat{(F^k)}_l(s) &= \frac{1}{\theta_l} \int_0^s \widehat{(\rho^k)}_l''(\omega) \sin\left(\theta_l(s-\omega)\right) d\omega, \\ \widehat{(F^k)}_l'(s) &= \int_0^s \widehat{(\rho^k)}_l''(\omega) \cos\left(\theta_l(s-\omega)\right) d\omega, \end{aligned} \tag{3.10}$$

where $\rho^k(x,s) = |E^k(x,s)|^2$ for $0 \le s \le \tau$, $a \le x \le b$, and $k \ge 0$. Setting $s = \tau$, using the same approach as in (2.16) and (2.17), we get

$$\begin{aligned} \widehat{(F^k)}_l(\tau) &= \frac{1}{\theta_l} \int_0^\tau \widehat{(\rho^k)}_l''(\omega) \sin\left(\theta_l(\tau-\omega)\right) d\omega \approx d_l\, \widehat{(\rho^k)}_l''(0), \\ \widehat{(F^k)}_l'(\tau) &= \int_0^\tau \widehat{(\rho^k)}_l''(\omega) \cos\left(\theta_l(\tau-\omega)\right) d\omega \approx \widehat{(\rho^k)}_l'(\tau) - \widehat{(\rho^k)}_l'(0) - b_l\theta_l \widehat{(\rho^k)}_l''(0). \end{aligned}$$

Let $F_j^{k,1}$, $\dot{F}_j^{k,1}$ be the approximations of $F^k(x_j,\tau)$ and $\partial_t F^k(x_j,\tau)$, respectively, for $j \in \mathcal{T}_M^0$ and $k \ge 0$. Using the same notation as in section 2.4, a TS-MTI for

computing E_j^{k+1}, $F_j^{k,1}$, and $\dot{F}_j^{k,1}$ reads for $j \in \mathcal{T}_M^0$, $k \geq 0$, as

$$
\begin{aligned}
&F_j^{k,1} = \sum_{l=1}^{M-1} d_l\, \widetilde{(\ddot{\rho}^k)}_l \sin\left(\frac{jl\pi}{M}\right), \quad E_j^{(1)} = \sum_{l=1}^{M-1} e^{-i\tau\mu_l^2/2}\, \widetilde{(E^k)}_l \sin\left(\frac{jl\pi}{M}\right),\\
&E_j^{(2)} = E_j^{(1)} e^{i\tau\left[|E_j^{(1)}|^2 - \frac{F_j^{k,1}}{2} - G_j^{k,\frac{1}{2}}\right]}, \quad E_j^{k+1} = \sum_{l=1}^{M-1} e^{-i\mu_l^2\frac{\tau}{2}}\, \widetilde{(E^{(2)})}_l \sin\left(\frac{jl\pi}{M}\right),\\
&\dot{F}_j^{k,1} = \sum_{l=1}^{M-1} \left[\widetilde{(\dot{\rho}^{k+1})}_l - \widetilde{(\dot{\rho}^k)}_l - b_l\,\theta_l\, \widetilde{(\ddot{\rho}^k)}_l\right] \sin\left(\frac{jl\pi}{M}\right),
\end{aligned}
\tag{3.11}
$$

where

$$
\begin{aligned}
&\rho_j^k = |E_j^k|^2, \quad \dot{\rho}_j^k = -2\,\mathrm{Im}\left(\overline{E_j^k} D_{xx} E_j^k\right), \quad \ddot{\rho}_j^k = -2\,\mathrm{Im}\left[\overline{\dot{E}_j^k}\, D_{xx} E_j^k + \overline{E_j^k}\, D_{xx}\dot{E}_j^k\right],\\
&G_j^{k,\frac{1}{2}} = \frac{1}{\tau}\int_0^\tau G^k(x_j, s)ds, \quad \dot{E}_j^k = i\left[D_{xx}E_j^k + \left(|E_j^k|^2 - G^k(x_j,0)\right)E_j^k\right].
\end{aligned}
$$

Again, noting (3.2), we have for $j \in \mathcal{T}_M^0$ and $k \geq 0$

$$
N_j^{k+1} = -|E_j^{k+1}|^2 + F_j^{k,1} + G^k(x_j,\tau), \quad \dot{N}_j^{k+1} = -\dot{\rho}_j^{k+1} + \dot{F}_j^{k,1} + \partial_s G^k(x_j,\tau). \tag{3.12}
$$

The TS-MTI method (3.11) for the ZS (2.6) is explicit, easy to be implemented, and very efficient due to the DST. The memory cost is $O(M)$, and the computational cost per time step is $O(M\log M)$. Moreover, it conserves the wave energy (2.32) in the discretized level.

4. Numerical results. In this section, we report numerical results to demonstrate the uniform convergence of the TS-EWI method and optimal convergence of the TS-MTI method for $\varepsilon \in (0,1]$. Furthermore, we apply the TS-MTI method to numerically study convergence rates of the ZS to its limiting models (1.5) and (2.5) in the subsonic limit regime.

4.1. Accuracy test. Two examples are presented to test the spatial/temporal accuracy for $\varepsilon \in (0,1]$. Let $E_\varepsilon^{\tau,h}$ and $N_\varepsilon^{\tau,h}$ be the numerical solution of (1.1) in 1D with mesh size h and time step τ. To quantify the numerical methods, we define the error functions as

$$
\begin{aligned}
&e_\varepsilon^{\tau,h}(T) := \frac{\|I_M(E_\varepsilon^{\tau,h}) - E(\cdot,T)\|_{H^1}}{\|E(\cdot,T)\|_{H^1}}, \quad n_\varepsilon^{\tau,h}(T) := \frac{\|I_M(N_\varepsilon^{\tau,h}) - N(\cdot,T)\|_{L^2}}{\|N(\cdot,T)\|_{L^2}},\\
&e_\infty^{\tau,h}(T) := \max_{0<\varepsilon\leq 1}\{e_\varepsilon^{\tau,h}(T)\}, \qquad\qquad n_\infty^{\tau,h}(T) := \max_{0<\varepsilon\leq 1}\{n_\varepsilon^{\tau,h}(T)\}.
\end{aligned}
$$

Example 1. The well-known solitary-wave solution of the ZS (1.1) with $d = 1$ is given in [29, 37] as

$$
\begin{aligned}
&E(x,t) = \sqrt{2B^2(1-C^2\varepsilon^2)}\,\mathrm{sech}(B(x-Ct))e^{i\left[(C/2)x - ((C/2)^2 - B^2)t\right]},\\
&N(x,t) = -2B^2\mathrm{sech}^2(B(x-Ct)), \quad x\in\mathbb{R}, \quad t\geq 0,
\end{aligned}
\tag{4.1}
$$

where B and C are constants. The initial condition is taken as

$$
E_0(x) = E(x,0), \quad N_0(x) = N(x,0), \quad N_1(x) = \partial_t N(x,0), \quad -\infty < x < \infty, \tag{4.2}
$$

TABLE 1
Spatial errors of the TS-EWI method at time $T = 1$ for Example 1.

$e_\varepsilon^{\tau,h}(1)$	$h = 1$	$h = 1/2$	$h = 1/4$	$h = 1/8$
$\varepsilon = 1/2$	9.20E-2	4.68E-4	1.17E-8	1.65E-12
$\varepsilon = 1/2^2$	1.05E-1	5.21E-4	1.15E-8	1.32E-12
$\varepsilon = 1/2^3$	1.09E-1	5.20E-4	1.12E-8	9.41E-13
$\varepsilon = 1/2^4$	1.10E-1	5.17E-3	1.14E-8	7.84E-13
$\varepsilon = 1/2^5$	1.10E-1	5.13E-3	1.15E-8	7.40E-13
$\varepsilon = 1/2^6$	1.10E-1	5.13E-3	1.15E-8	7.09E-13
$\varepsilon = 1/2^{10}$	1.10E-1	5.13E-3	1.15E-8	7.10E-13
$\varepsilon = 1/2^{20}$	1.10E-1	5.13E-3	1.15E-8	7.09E-13
$n_\varepsilon^{\tau,h}(1)$	$h = 1$	$h = 1/2$	$h = 1/4$	$h = 1/8$
$\varepsilon = 1/2$	5.72E-2	6.15E-4	1.02E-8	2.09E-12
$\varepsilon = 1/2^2$	4.76E-2	3.08E-4	4.14E-9	9.01E-13
$\varepsilon = 1/2^3$	4.08E-2	2.07E-4	4.37E-9	6.63E-13
$\varepsilon = 1/2^4$	3.96E-2	1.86E-4	2.89E-9	5.59E-13
$\varepsilon = 1/2^5$	3.94E-2	1.84E-4	2.30E-9	3.34E-13
$\varepsilon = 1/2^6$	3.94E-2	1.83E-4	2.26E-9	5.76E-13
$\varepsilon = 1/2^{10}$	3.94E-2	1.83E-4	2.29E-9	5.85E-13
$\varepsilon = 1/2^{20}$	3.94E-2	1.83E-4	2.29E-9	5.80E-13

where $E(x,0)$, $N(x,0)$, $N_t(x,0)$ are obtained from (4.1) by setting $t = 0$. Here we choose $B = C = 1$ in (4.1) and test spatial and temporal discretization errors. The problem is solved on the interval $[-32, 32]$ with homogeneous Dirichlet boundary conditions by using either TS-EWI or TS-MTI.

Table 1 shows the spatial errors of the TS-EWI method at $T = 1$ under different ε and h with a very small time step $\tau = 10^{-6}$ such that the discretization error in time is negligible. The results for the TS-MTI method are similar, which are omitted here for brevity. Tables 2 and 3 display the temporal errors at $T = 1$ with a fixed mesh size $h = 1/16$ for the TS-EWI and TS-MTI methods, respectively. It can be clearly observed that for solitary-wave solution, both TS-EWI and TS-MTI methods converge uniformly and optimally for $\varepsilon \in (0, 1]$ in both space and time with exponential and quadratic convergence rates, respectively. Furthermore, generally speaking, the TS-MTI method is superior to the TS-EWI method in accuracy for fixed ε and τ, especially when $\varepsilon \geq \varepsilon_0 = 1/2^5$.

Example 2. The initial data of the ZS (1.1) is chosen as

$$E_0(x) = e^{-x^2/2}, \quad N_0(x) = -|E_0(x)|^2 + \varepsilon^\alpha \omega_0(x), \quad N_1(x) = \varepsilon^\beta e^{-x^2/3} \sin(2x),$$
$$\omega_0(x) = g\left(\frac{x+25}{10}\right) g\left(\frac{25-x}{10}\right) \sin(2x), \qquad x \in \mathbb{R},$$

where $\alpha \geq 0$ and $\beta \geq -1$ are two parameters describing the incompatibility of the initial data of the ZS (1.1) with respect to the limiting NLSE (1.5) and g is given in (1.9).

Since the analytical solution of the problem is not available, the "reference" solution is obtained numerically by the TS-MTI method with a very fine mesh size $h = 1/64$ and a small time step $\tau = 10^{-6}$. By using TS-EWI, the problem is truncated on a bounded interval $\Omega_\varepsilon = [-30 - \frac{1}{\varepsilon}, 30 + \frac{1}{\varepsilon}]$, which is large enough such that the homogeneous Dirichlet boundary condition does not introduce significant errors. On the contrary, by using TS-MTI, it is enough to truncate the problem on a bounded interval $\Omega = [-32, 32]$, which is ε-independent.

TABLE 2
Temporal errors of the TS-EWI method for Example 1.

$e_\varepsilon^{\tau,h}(1)$	$\tau_0 = 0.2$	$\tau_0/4$	$\tau_0/4^2$	$\tau_0/4^3$	$\tau_0/4^4$	$\tau_0/4^5$	$\tau_0/4^6$
$\varepsilon = 1/2$	8.47E-2	1.48E-2	1.11E-3	7.10E-5	4.45E-6	2.78E-7	1.74E-8
rate	-	1.26	1.87	1.99	2.00	2.00	2.00
$\varepsilon = 1/2^3$	3.26E-2	3.04E-3	2.13E-4	1.36E-5	8.55E-7	5.35E-8	3.34E-9
rate	-	1.71	1.92	1.98	2.00	2.00	2.00
$\varepsilon = 1/2^5$	2.85E-2	1.76E-3	1.13E-4	7.25E-6	4.56E-7	2.86E-8	1.79E-9
rate	-	2.01	1.98	1.98	1.99	2.00	2.00
$\varepsilon = 1/2^7$	2.81E-2	1.76E-3	1.09E-4	6.85E-6	4.31E-7	2.70E-8	1.69E-9
rate	-	2.00	2.00	2.00	2.00	2.00	2.00
$\varepsilon = 1/2^9$	2.81E-2	1.75E-3	1.10E-4	6.87E-6	4.30E-7	2.69E-8	1.68E-9
rate	-	2.00	2.00	2.00	2.00	2.00	2.00
$\varepsilon = 1/2^{11}$	2.81E-2	1.75E-3	1.10E-4	6.89E-6	4.30E-7	2.69E-8	1.68E-9
rate	-	2.00	2.00	2.00	2.00	2.00	2.00
$\varepsilon = 1/2^{15}$	2.81E-2	1.75E-3	1.10E-4	6.89E-6	4.31E-7	2.69E-8	1.68E-9
rate	-	2.00	2.00	2.00	2.00	2.00	2.00
$n_\varepsilon^{\tau,h}(1)$	$\tau_0 = 0.2$	$\tau_0/4$	$\tau_0/4^2$	$\tau_0/4^3$	$\tau_0/4^4$	$\tau_0/4^5$	$\tau_0/4^6$
$\varepsilon = 1/2$	1.15E-1	2.32E-2	1.84E-3	1.18E-4	7.40E-6	4.63E-7	2.89E-8
rate	-	1.15	1.83	1.98	2.00	2.00	2.00
$\varepsilon = 1/2^3$	2.63E-2	2.46E-3	1.78E-4	1.14E-5	7.14E-7	4.47E-8	2.79E-9
rate	-	1.71	1.90	1.98	2.00	2.00	2.00
$\varepsilon = 1/2^5$	1.25E-2	8.66E-4	7.27E-5	3.60E-6	2.28E-7	1.43E-8	8.94E-10
rate	-	1.93	1.79	2.17	1.99	2.00	2.00
$\varepsilon = 1/2^7$	1.20E-2	8.16E-4	4.92E-5	3.17E-6	2.01E-7	1.26E-8	7.88E-10
rate	-	1.94	2.03	1.98	1.99	2.00	2.00
$\varepsilon = 1/2^9$	1.20E-2	8.13E-4	5.10E-5	3.10E-6	1.99E-7	1.25E-8	7.81E-10
rate	-	1.94	2.00	2.02	1.98	2.00	2.00
$\varepsilon = 1/2^{11}$	1.20E-2	8.13E-4	5.11E-5	3.19E-6	1.94E-7	1.25E-8	7.80E-10
rate	-	1.94	2.00	2.00	2.02	1.98	2.00
$\varepsilon = 1/2^{13}$	1.20E-2	8.13E-4	5.11E-5	3.20E-6	1.99E-7	1.22E-8	7.80E-10
rate	-	1.94	2.00	2.00	2.00	2.02	1.98
$\varepsilon = 1/2^{15}$	1.20E-2	8.13E-4	5.11E-5	3.19E-6	2.00E-7	1.25E-8	7.61E-10
rate	-	1.94	2.00	2.00	2.00	2.00	2.02

The spatial discretization errors for the TS-EWI and TS-MTI methods behave similarly to Table 1, and thus they are omitted here for brevity. Table 4 shows the temporal discretization errors of the TS-EWI method at $T = 1$ with a fixed mesh size $h = 1/8$ for $\alpha = 1$ and $\beta = 0$, and, respectively, Table 5 displays that for $\alpha = \beta = 0$. Figure 6 plots the temporal errors of the TS-MTI method at $T = 1$ with a fixed mesh size $h = 1/8$ for $\alpha = 1$ and $\beta = 0$, Figure 7 depicts similar results for $\alpha = \beta = 0$, and Figure 8 displays temporal errors for larger time $T = 5$ for $\alpha = 0$ and $\beta = -1$.

From Tables 4 and 5 and Figures 6–8, we can draw the following observations:

(i) Both TS-EWI and TS-MTI converge uniformly and optimally at exponential order in space for any kind of initial data.

(ii) The TS-MTI method converges uniformly and optimally at second order in time for all kinds of initial data (cf. Figures 6–8).

(iii) The TS-EWI method converges uniformly and optimally at second order in time when $\alpha \geq 1$ and $\beta \geq 0$ (cf. Table 4). However, when $0 \leq \alpha < 1$ and/or $-1 \leq \beta < 0$, it converges uniformly but not optimally at second order in time (cf. Table 5).

4.2. Convergence rates of the ZS to its limiting models when $\varepsilon \to 0$. Here we apply the TS-MTI method to study numerically convergence rate of the ZS

TABLE 3
Temporal errors of the TS-MTI method for Example 1.

$e_\varepsilon^{\tau,h}(1)$	$\tau_0 = 0.2$	$\tau_0/4$	$\tau_0/4^2$	$\tau_0/4^3$	$\tau_0/4^4$	$\tau_0/4^5$	$\tau_0/4^6$
$\varepsilon = 1/2$	4.17E-2	3.51E-3	2.31E-4	1.46E-5	9.12E-7	5.70E-8	3.57E-9
rate	-	1.78	1.96	1.99	2.00	2.00	2.00
$\varepsilon = 1/2^3$	2.95E-2	1.51E-3	9.18E-5	5.74E-6	3.59E-7	2.24E-8	1.40E-9
rate	-	2.14	2.02	2.00	2.00	2.00	2.00
$\varepsilon = 1/2^5$	2.89E-2	1.70E-3	7.86E-5	4.73E-6	2.95E-7	1.84E-8	1.15E-9
rate	-	2.05	2.21	2.03	2.00	2.00	2.00
$\varepsilon = 1/2^7$	2.82E-2	1.80E-3	1.05E-4	4.85E-6	2.92E-7	1.82E-8	1.14E-9
rate	-	1.99	2.05	2.22	2.03	2.00	2.00
$\varepsilon = 1/2^9$	2.81E-2	1.76E-3	1.13E-4	6.58E-6	3.03E-7	1.82E-8	1.14E-9
rate	-	2.00	1.98	2.05	2.22	2.03	2.00
$\varepsilon = 1/2^{11}$	2.81E-2	1.75E-3	1.10E-4	7.05E-6	4.11E-7	1.89E-8	1.14E-9
rate	-	2.00	2.00	1.98	2.05	2.22	2.03
$\varepsilon = 1/2^{13}$	2.81E-2	1.75E-3	1.10E-4	6.90E-6	4.41E-7	2.57E-8	1.18E-9
rate	-	2.00	2.00	2.00	1.98	2.05	2.22
$\varepsilon = 1/2^{15}$	2.81E-2	1.75E-3	1.10E-4	6.89E-6	4.31E-7	2.75E-8	1.61E-9
rate	-	2.00	2.00	2.00	2.00	1.98	2.05
$n_\varepsilon^{\tau,h}(1)$	$\tau_0 = 0.2$	$\tau_0/4$	$\tau_0/4^2$	$\tau_0/4^3$	$\tau_0/4^4$	$\tau_0/4^5$	$\tau_0/4^6$
$\varepsilon = 1/2$	5.60E-2	5.05E-3	3.31E-4	2.08E-5	1.30E-6	8.13E-8	5.08E-9
rate	-	1.73	1.97	2.00	2.00	2.00	2.00
$\varepsilon = 1/2^3$	1.86E-2	1.11E-3	6.87E-5	4.30E-6	2.69E-7	1.68E-8	1.05E-9
rate	-	2.03	2.01	2.00	2.00	2.00	2.00
$\varepsilon = 1/2^5$	1.29E-2	8.57E-4	3.32E-5	1.74E-6	1.06E-7	6.64E-9	4.16E-10
rate	-	1.96	2.34	2.13	2.02	2.00	2.00
$\varepsilon = 1/2^7$	1.20E-2	8.40E-4	5.14E-5	1.94E-6	1.06E-7	6.46E-9	4.02E-10
rate	-	1.92	2.02	2.36	2.10	2.02	2.00
$\varepsilon = 1/2^9$	1.20E-2	8.15E-4	5.26E-5	3.17E-6	1.15E-7	6.48E-9	4.01E-10
rate	-	1.94	1.98	2.03	2.39	2.07	2.01
$\varepsilon = 1/2^{11}$	1.20E-2	8.13E-4	5.12E-5	3.29E-6	1.97E-7	7.08E-9	4.04E-10
rate	-	1.94	1.99	1.98	2.03	2.40	2.07
$\varepsilon = 1/2^{13}$	1.20E-2	8.13E-4	5.11E-5	3.20E-6	2.06E-7	1.23E-8	4.42E-10
rate	-	1.94	2.00	2.00	1.98	2.03	2.40
$\varepsilon = 1/2^{15}$	1.20E-2	8.13E-4	5.11E-5	3.19E-6	2.00E-7	1.29E-8	7.71E-10
rate	-	1.94	2.00	2.00	2.00	1.98	2.03

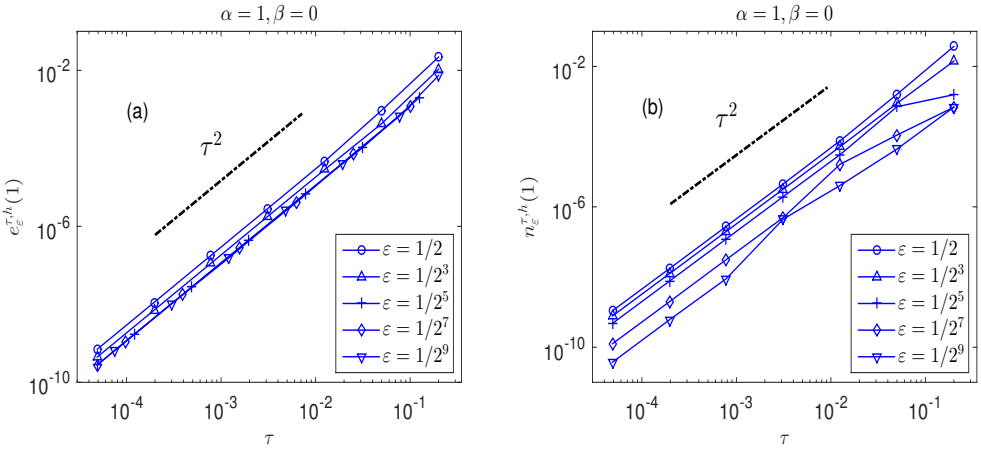

FIG. 6. *Temporal errors of the TS-MTI method for Example* 2 *with* $\alpha = 1$, $\beta = 0$.

TABLE 4
Temporal errors of the TS-EWI method for Example 2 with $\alpha = 1$, $\beta = 0$.

$e_\varepsilon^{\tau,h}(1)$	$\tau_0 = 0.2$	$\tau_0/2$	$\tau_0/2^2$	$\tau_0/2^3$	$\tau_0/2^4$	$\tau_0/2^5$	$\tau_0/2^6$	$\tau_0/2^7$
$\varepsilon = 1/2$	3.28E-2	1.37E-2	4.27E-3	1.15E-3	2.95E-4	7.44E-5	1.86E-5	4.66E-6
rate	-	1.26	1.68	1.89	1.97	1.99	2.00	2.00
$\varepsilon = 1/2^3$	1.13E-2	1.98E-3	5.10E-4	1.30E-4	3.25E-5	8.15E-6	2.04E-6	5.09E-7
rate	-	2.52	1.96	1.98	1.99	2.00	2.00	2.00
$\varepsilon = 1/2^5$	7.47E-3	1.26E-3	2.88E-4	7.17E-5	1.79E-5	4.48E-6	1.12E-6	2.80E-7
rate	-	2.56	2.13	2.01	2.00	2.00	2.00	2.00
$\varepsilon = 1/2^7$	7.37E-3	1.16E-3	2.81E-4	7.08E-5	1.74E-5	4.37E-6	1.09E-6	2.73E-7
rate	-	2.67	2.04	1.99	2.02	1.99	2.00	2.00
$\varepsilon = 1/2^9$	7.36E-3	1.15E-3	2.80E-4	6.99E-5	1.75E-5	4.37E-6	1.09E-6	2.73E-7
rate	-	2.67	2.04	2.00	2.00	2.00	2.00	2.00
$n_\varepsilon^{\tau,h}(1)$	$\tau_0 = 0.2$	$\tau_0/2$	$\tau_0/2^2$	$\tau_0/2^3$	$\tau_0/2^4$	$\tau_0/2^5$	$\tau_0/2^6$	$\tau_0/2^7$
$\varepsilon = 1/2$	5.13E-2	2.09E-2	6.62E-3	1.85E-3	4.83E-4	1.22E-4	3.07E-5	7.67E-6
rate	-	1.30	1.66	1.83	1.94	1.98	2.00	2.00
$\varepsilon = 1/2^2$	4.16E-2	1.24E-2	3.23E-3	8.15E-4	2.05E-4	5.12E-5	1.28E-5	3.20E-6
rate	-	1.75	1.94	1.98	2.00	2.00	2.00	2.00
$\varepsilon = 1/2^3$	6.01E-2	4.90E-3	3.46E-4	8.16E-5	2.00E-5	4.97E-6	1.24E-6	3.09E-7
rate	-	3.62	3.82	2.08	2.03	2.01	2.00	2.00
$\varepsilon = 1/2^4$	3.62E-3	2.87E-2	1.36E-3	1.01E-4	2.38E-5	5.88E-6	1.46E-6	3.66E-7
rate	-	-2.98	4.40	3.75	2.09	2.02	2.01	2.00
$\varepsilon = 1/2^5$	1.13E-3	5.86E-4	8.40E-3	2.57E-4	1.66E-5	3.92E-6	9.67E-7	2.41E-7
rate	-	0.95	-3.84	5.03	3.95	2.08	2.02	2.00
$\varepsilon = 1/2^6$	8.18E-4	1.94E-4	8.59E-5	1.72E-3	4.60E-5	2.20E-6	5.19E-7	1.28E-7
rate	-	2.08	1.17	-4.33	5.23	4.39	2.08	2.02
$\varepsilon = 1/2^7$	7.28E-4	1.55E-4	4.01E-5	1.46E-5	3.21E-4	8.05E-6	3.02E-7	7.19E-8
rate	-	2.23	1.95	1.45	-4.45	5.32	4.74	2.07
$\varepsilon = 1/2^8$	6.73E-4	1.50E-4	3.65E-5	9.41E-6	2.91E-6	5.79E-5	1.42E-6	4.88E-8
rate	-	2.17	2.04	1.95	1.69	-4.31	5.35	4.86
$\varepsilon = 1/2^9$	6.41E-4	1.48E-4	3.63E-5	9.03E-6	2.30E-6	6.42E-7	1.03E-5	2.50E-7
rate	-	2.12	2.03	2.01	1.97	1.84	-4.01	5.37
$n_\infty^{\tau,h}(1)$	6.01E-2	2.87E-2	8.40E-3	1.85E-3	4.83E-4	1.22E-4	3.07E-5	7.67E-5
rate	-	1.07	1.77	2.18	1.94	1.99	1.99	2.00

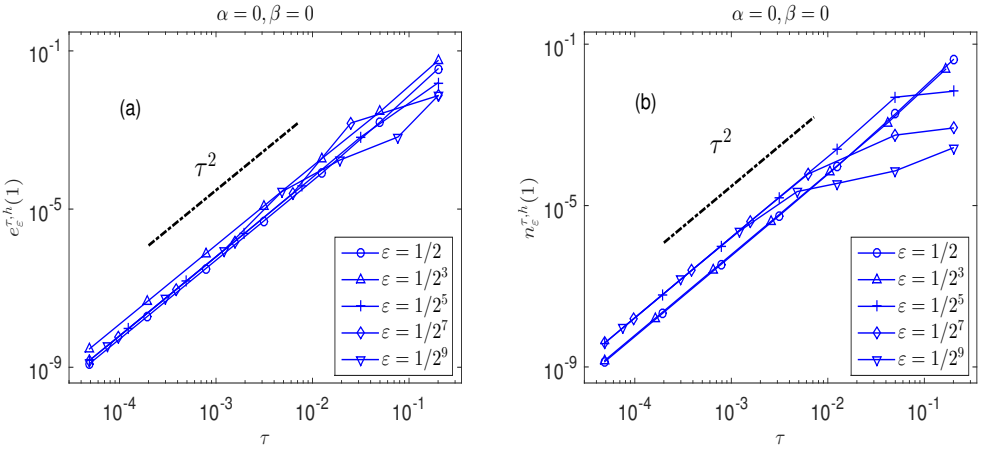

FIG. 7. *Temporal errors of the TS-MTI method for Example 2 with $\alpha = \beta = 0$.*

TABLE 5
Temporal errors of the TS-EWI method for Example 2 with $\alpha = \beta = 0$.

$e_\varepsilon^{\tau,h}(1)$	$\tau_0 = 0.2$	$\tau_0/2$	$\tau_0/2^2$	$\tau_0/2^3$	$\tau_0/2^4$	$\tau_0/2^5$	$\tau_0/2^6$	$\tau_0/2^7$
$\varepsilon = 1/2^2$	3.51E-2	9.92E-3	2.98E-3	7.98E-4	2.03E-4	5.11E-5	1.28E-5	3.20E-6
rate	-	1.82	1.74	1.90	1.97	1.99	2.00	2.00
$\varepsilon = 1/2^3$	5.70E-2	1.05E-2	2.55E-3	6.37E-4	1.59E-4	3.98E-5	9.95E-6	2.49E-6
rate	-	2.44	2.04	2.00	2.00	2.00	2.00	2.00
$\varepsilon = 1/2^4$	3.01E-2	1.01E-2	2.07E-3	5.01E-4	1.24E-4	3.10E-5	7.75E-6	1.94E-6
rate	-	1.57	2.29	2.05	2.01	2.00	2.00	2.00
$\varepsilon = 1/2^5$	1.56E-2	1.38E-2	1.93E-3	4.06E-4	9.82E-5	2.44E-5	6.08E-6	1.52E-6
rate	-	0.17	2.84	2.25	2.05	2.01	2.00	2.00
$\varepsilon = 1/2^6$	8.65E-3	5.54E-3	5.34E-3	4.63E-4	1.01E-4	2.44E-5	6.04E-6	1.51E-6
rate	-	0.64	0.05	3.53	2.20	2.05	2.01	2.00
$\varepsilon = 1/2^7$	7.37E-3	1.65E-3	1.56E-3	1.49E-3	1.18E-4	2.51E-5	6.08E-6	1.51E-6
rate	-	2.16	0.08	0.06	3.66	2.24	2.05	2.01
$\varepsilon = 1/2^8$	7.36E-3	1.15E-3	4.06E-4	4.01E-4	3.83E-4	3.02E-5	6.28E-6	1.52E-6
rate	-	2.67	1.51	0.02	0.07	3.66	2.27	2.05
$\varepsilon = 1/2^9$	7.36E-3	1.15E-3	2.80E-4	1.01E-4	1.01E-4	9.64E-5	7.60E-6	1.57E-6
rate	-	2.67	2.04	1.47	0.01	0.07	3.66	2.28
$\varepsilon = 1/2^{10}$	7.36E-3	1.15E-3	2.80E-4	6.99E-5	2.54E-5	2.53E-5	2.41E-5	1.90E-6
rate	-	2.67	2.04	2.00	1.46	0.00	0.07	3.66
$e_\infty^{\tau,h}(1)$	5.70E-2	1.38E-2	5.34E-3	1.49E-3	3.83E-4	9.64E-5	2.41-5	6.03E-6
rate	-	2.05	1.37	1.84	1.96	1.99	2.00	2.00
$n_\varepsilon^{\tau,h}(1)$	$\tau_0 = 0.2$	$\tau_0/2$	$\tau_0/2^2$	$\tau_0/2^3$	$\tau_0/2^4$	$\tau_0/2^5$	$\tau_0/2^6$	$\tau_0/2^7$
$\varepsilon = 1/2$	5.33E-2	2.05E-2	6.29E-3	1.78E-3	4.68E-4	1.19E-4	2.98E-5	7.46E-6
rate	-	1.38	1.70	1.82	1.93	1.98	1.99	2.00
$\varepsilon = 1/2^2$	6.65E-2	2.40E-2	6.69E-3	1.73E-3	4.36E-4	1.09E-4	2.73E-5	6.83E-6
rate	-	1.47	1.84	1.96	1.99	2.00	2.00	2.00
$\varepsilon = 1/2^3$	1.20E-1	3.72E-3	4.69E-4	1.17E-4	2.94E-5	7.36E-6	1.84E-6	4.60E-7
rate	-	5.01	2.98	2.00	1.99	2.00	2.00	2.00
$\varepsilon = 1/2^4$	1.05E-2	1.19E-1	2.36E-3	4.01E-4	9.50E-5	2.35E-5	5.84E-6	1.46E-6
rate	-	-3.50	5.66	2.56	2.08	2.02	2.00	2.00
$\varepsilon = 1/2^5$	3.36E-3	3.44E-3	7.06E-2	7.48E-4	1.35E-4	3.19E-5	7.88E-6	1.96E-6
rate	-	-0.03	-4.36	6.56	2.47	2.08	2.02	2.00
$\varepsilon = 1/2^6$	9.67E-4	8.78E-4	8.70E-4	2.88E-2	2.18E-4	3.45E-5	8.18E-6	2.02E-6
rate	-	0.14	0.01	-5.05	7.05	2.66	2.08	2.02
$\varepsilon = 1/2^7$	4.17E-4	3.45E-4	2.29E-4	2.15E-4	1.07E-2	6.60E-5	8.68E-6	2.05E-6
rate	-	0.28	0.59	0.09	-5.64	7.34	2.93	2.08
$\varepsilon = 1/2^8$	2.16E-4	1.47E-4	1.20E-4	6.23E-5	5.40E-5	3.86E-3	2.09E-5	2.18E-6
rate	-	0.55	0.29	0.95	0.21	-6.16	7.53	3.26
$\varepsilon = 1/2^9$	1.73E-4	6.23E-5	5.18E-5	4.17E-5	1.78E-5	1.38E-5	1.38E-3	6.89E-6
rate	-	1.47	0.27	0.31	1.23	0.37	-6.65	7.64
$\varepsilon = 1/2^{10}$	1.63E-4	4.19E-5	2.01E-5	1.82E-5	1.45E-5	5.39E-6	3.58E-6	4.90E-4
rate	-	1.96	1.06	0.15	0.32	1.43	0.59	-7.10
$n_\infty^{\tau,h}(1)$	1.20E-1	1.19E-1	7.06E-2	2.88E-2	1.07E-2	3.86E-3	1.38E-3	4.90E-4
rate	-	0.01	0.75	1.29	1.43	1.47	1.48	1.49

(1.1) to its limiting model—the NLSE (1.5) and its semilimiting model—the NLSE-OP (2.5). In order to do so, we take $d = 1$ in (1.1) and choose the same initial data as in Example 2.

Let (E, N) be the solution of the ZS (1.1) which is obtained numerically by the TS-MTI method (3.11) on a bounded interval $\Omega = [-32, 32]$ with a very fine mesh $h = 1/16$ and a small time step $\tau = 10^{-4}$. Similarly, let $E_{\rm s}$ and $E_{\rm sop}$ be the solutions of the NLSE (1.5) and the NLSE-OP (2.5), respectively, which are obtained numerically on Ω by the time-splitting sine pseudospectral method with $h = 1/16$ and $\tau = 10^{-4}$.

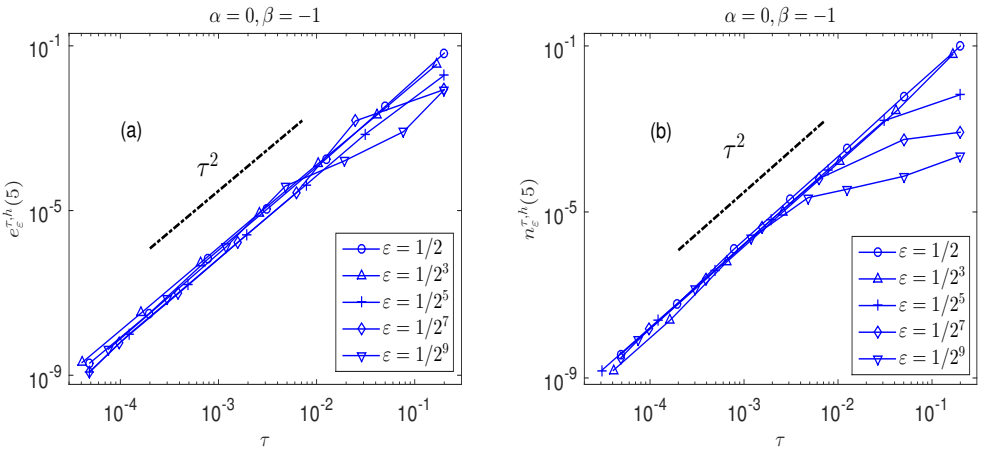

FIG. 8. *Temporal errors of the TS-MTI method for Example* 2 *for* $T = 5$.

Denote $N_{\rm s}(x,t) = -|E_{\rm s}|^2 + G(x,t)$ and $N_{\rm sop}(x,t) = -|E_{\rm sop}|^2 + G(x,t)$ with $G(x,t)$ being the solution of the wave equation (2.1) with initial data (2.2). Define the error functions as

$$\eta_{\rm se}(t) := \|E(\cdot,t) - E_{\rm s}(\cdot,t)\|_{H^1}, \quad \eta_{_F}(t) := \|N(\cdot,t) + |E(\cdot,t)|^2 - G(\cdot,t)\|_{L^2},$$
$$\eta_{\rm sope}(t) := \|E(\cdot,t) - E_{\rm sop}(\cdot,t)\|_{H^1}, \quad \eta_{\rm sopn}(t) := \|N(\cdot,t) - N_{\rm sop}(\cdot,t)\|_{L^2}.$$

Figure 9 plots the errors between the solutions of the ZS (1.1) and the NLSE (1.5), i.e., $\eta_{\rm se}(t)$ and $\eta_{_F}(t)$, with compatible initial data, i.e., $\omega_0(x) \equiv 0$ and $\omega_1(x) \equiv 0$ in (1.7) for different $\varepsilon > 0$; Figures 10 and 11 show similar results for $\alpha = 1$, $\beta = 0$ and $\alpha = 0$, $\beta = -1$ in (1.7), respectively. Finally, Figure 12 depicts the errors between the solutions of the ZS (1.1) and the NLSE-OP (2.5), i.e., $\eta_{\rm sope}(t)$ and $\eta_{\rm sopn}(t)$, for ill-prepared initial data, i.e., $\alpha = 0$, $\beta = -1$ in (1.7).

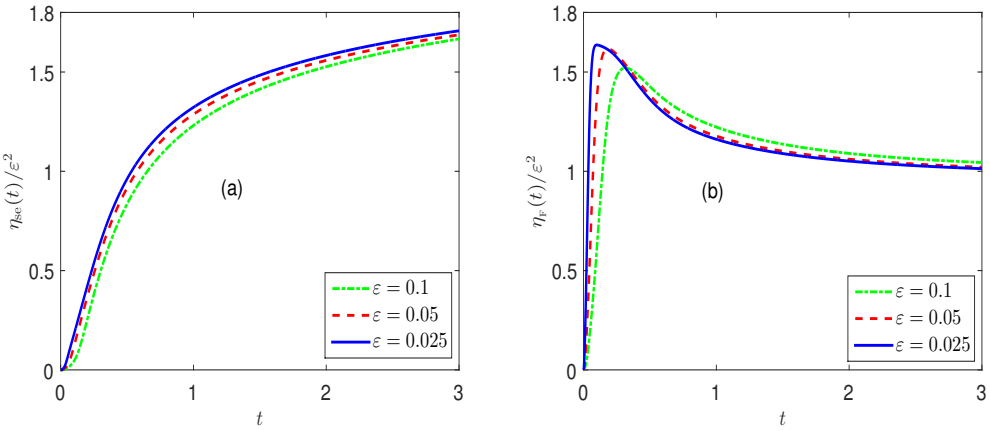

FIG. 9. *Convergence behavior between the ZS* (1.1) *and the NLSE* (1.5) *under compatible initial data* (1.7)*, i.e.,* $\omega_0 = \omega_1 \equiv 0$.

From Figures 9–12, we can draw the following conclusions:

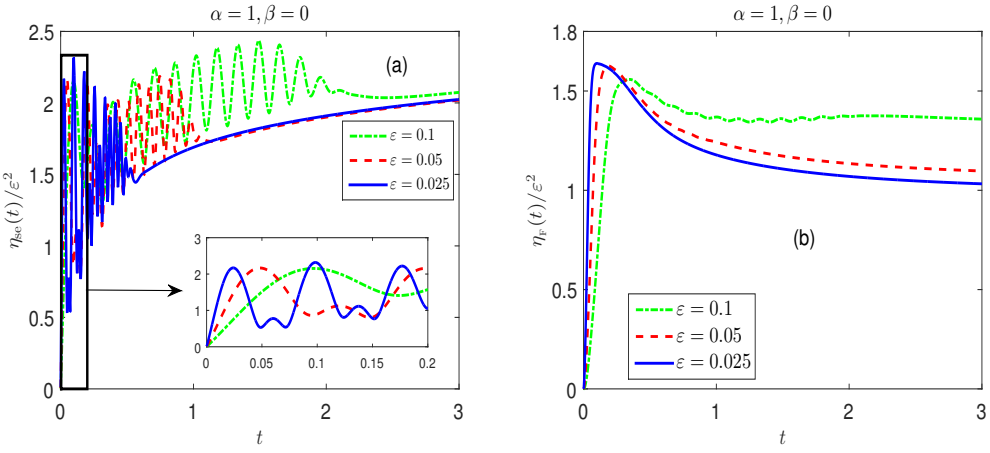

FIG. 10. *Convergence behavior between the ZS* (1.1) *and the NLSE* (1.5) *under less ill-prepared initial data* (1.7)*, i.e.,* $\alpha = 1$*,* $\beta = 0$*.*

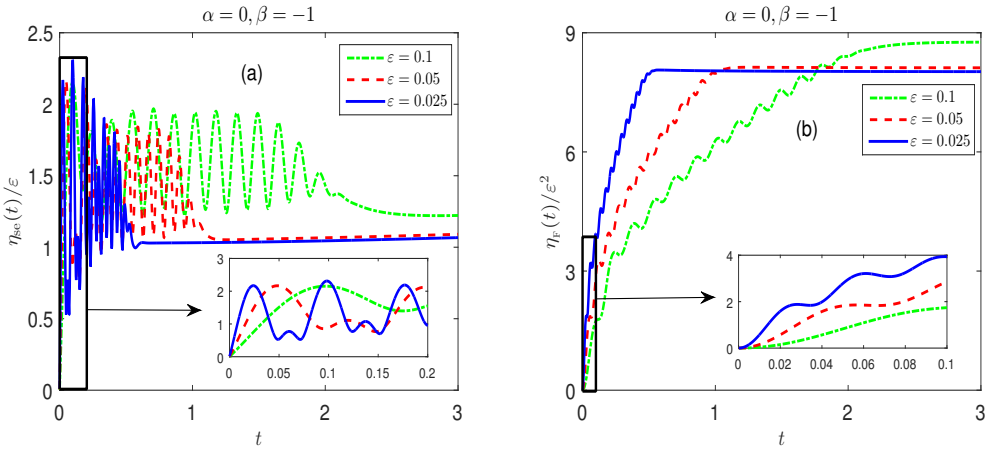

FIG. 11. *Convergence behavior between the ZS* (1.1) *and the NLSE* (1.5) *under ill-prepared initial data* (1.7)*, i.e.,* $\alpha = 0$*,* $\beta = -1$*.*

(i) The solution E of the ZS (1.1) converges to $E_{\rm s}$ of the NLSE (1.5), and N converges to $N_{\rm s}$ when $\varepsilon \to 0^+$. In addition, we have the following convergence rates:

$$\begin{aligned} &\|E(\cdot,t) - E_{\rm s}(\cdot,t)\|_{H^1} + \|N(\cdot,t) - N_{\rm s}(\cdot,t)\|_{L^2} \le C_0 \varepsilon^{\min\{2,1+\alpha,2+\beta\}}, \\ &\|F(\cdot,t)\|_{L^2} = \|N(\cdot,t) + |E(\cdot,t)|^2 - G(\cdot,t)\|_{L^2} \le C_1 \varepsilon^2, \quad 0 \le t \le T, \end{aligned} \tag{4.3}$$

where C_0 and C_1 are two positive constants which are independent of $\varepsilon \in (0, 1]$, which is consistent with the analytical results in [38].

(ii) The solution E of the ZS (1.1) converges to $E_{\rm sop}$ of the NLSE-OP (2.5), and N converges to $N_{\rm sop}$ when $\varepsilon \to 0^+$. In addition, we have the following (uniformly) quadratic convergence rate for any kind of initial data:

$$\|E(\cdot,t) - E_{\rm sop}(\cdot,t)\|_{H^1} + \|N(\cdot,t) - N_{\rm sop}(\cdot,t)\|_{L^2} \le C_2 \varepsilon^2, \quad 0 \le t \le T, \tag{4.4}$$

where $C_2 > 0$ is a constant independent of ε. Based on the above results, we can see

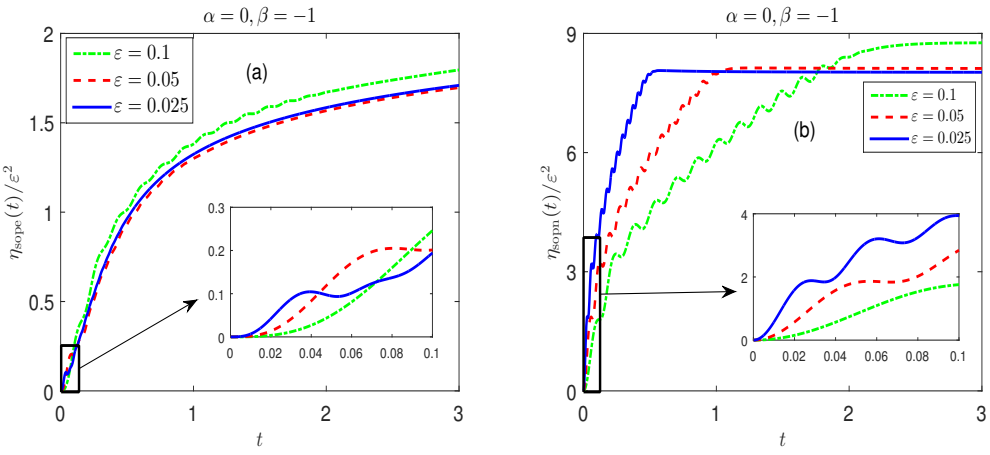

FIG. 12. *Convergence behavior between the ZS* (1.1) *and the NLSE-OP* (2.5) *under ill-prepared initial data* (1.7)*, i.e.,* $\alpha = 0$*,* $\beta = -1$*.*

that the NLSE-OP (2.5) is a more accurate limiting model to approximate the ZS in the subsonic limit, compared to the NLSE (1.5), especially for ill-prepared initial data.

5. Conclusion. Two uniformly accurate numerical methods were proposed for the Zakharov system (ZS) with a dimensionless parameter $0 < \varepsilon \leq 1$ which is inversely proportional to the acoustic speed. The time-splitting exponential wave integrator (TS-EWI) method was designed by adopting an asymptotic consistent formulation of the ZS, and the time-splitting multiscale time integrator (TS-MTI) method was proposed by introducing a multiscale decomposition of the solution of the ZS. Both methods are explicit and uniformly and optimally accurate (UOA) at spectral order in space. The TS-MTI method is uniformly and optimally accurate at second order in time for all kinds of initial data, while the TS-EWI is UOA at second order in time for reasonably well-prepared initial data. Another advantage of the TS-MTI method is that the bounded computational domain can be taken as ε-independent, while the bounded computational domain for the TS-EWI method needs to be taken as ε-dependent, especially when $\tau = O(\varepsilon)$ and $0 < \varepsilon \ll 1$. By adopting our numerical method, we observed numerically that the nonlinear Schrödinger equation (NLSE) with an oscillatory potential is a more accurate limiting model to the ZS in the subsonic limit, compared to the NLSE with cubic nonlinearity, especially for ill-prepared initial data.

REFERENCES

[1] W. Bao, Y. Cai, and X. Zhao, *A uniformly accurate multiscale time integrator pseudospectral method for the Klein–Gordon equation in the nonrelativistic limit regime*, SIAM J. Numer. Anal., 52 (2014), pp. 2488–2511, https://doi.org/10.1137/130950665.

[2] W. Bao and X. Dong, *Analysis and comparison of numerical methods for Klein-Gordon equation in nonrelativistic limit regime*, Numer. Math., 120 (2012), pp. 189–229.

[3] W. Bao, X. Dong, and X. Zhao, *Uniformly accurate multiscale time integrators for highly oscillatory second order differential equations*, J. Math. Study, 47 (2014), pp. 111–150.

[4] W. Bao, D. Jaksch, and P. A. Markowich, *Numerical solution of the Gross-Pitaevskii equation for Bose-Einstein condensation*, J. Comput. Phys., 187 (2003), pp. 318–342.

[5] W. Bao, S. Jin, and P. A. Markowich, *On time-splitting spectral approximation for the*

Schrödinger equation in the semiclassical regime, J. Comput. Phys., 175 (2002), pp. 487–524.

[6] W. Bao and C. Su, *Uniform error bounds of a finite difference method for the Zakharov system in the subsonic limit regime via an asymptotic consistent formulation*, Multiscale Model. Simul., 15 (2017), pp. 977–1002, https://doi.org/10.1137/16M1078112.

[7] W. Bao and F. Sun, *Efficient and stable numerical methods for the generalized and vector Zakharov system*, SIAM J. Sci. Comput., 26 (2005), pp. 1057–1088, https://doi.org/10.1137/030600941.

[8] W. Bao, F. Sun, and G. W. Wei, *Numerical methods for the generalized Zakharov system*, J. Comput. Phys., 190 (2003), pp. 201–228.

[9] J. Berenger, *A perfectly matched layer for the absorption of electromagnetic waves*, J. Comput. Phys., 114 (1994), pp. 185–200.

[10] C. Besse, B. Bidégaray, and S. Descombes, *Order estimates in time of splitting methods for the nonlinear Schrödinger equation*, SIAM J. Numer. Anal., 40 (2002), pp. 26–40, https://doi.org/10.1137/S0036142900381497.

[11] A. H. Bhrawy, *An efficient Jacobi pseudospectral approximation for nonlinear complex generalized Zakharov system*, Appl. Math. Comput., 247 (2014), pp. 30–46.

[12] J. Bourgain and J. Colliander, *On well-posedness of the Zakharov system*, Internat. Math. Res. Notices, 11 (1996), pp. 515–546.

[13] Y. Cai and Y. Yuan, *Uniform error estimates of the conservative finite difference method for the Zakharov system in the subsonic limit regime*, Math. Comp., 87 (2018), pp. 1191–1225.

[14] Q. Chang, B. Guo, and H. Jiang, *Finite difference method for generalized Zakharov equations*, Math. Comp., 64 (1995), pp. 537–553.

[15] Q. Chang and H. Jiang, *A conservative difference scheme for the Zakharov equations*, J. Comput. Phys., 113 (1994), pp. 309–319.

[16] J. Colliander, *Well-posedness for Zakharov systems with generalized nonlinearity*, J. Differential Equations, 148 (1998), pp. 351–363.

[17] A. S. Davydov, *Solitons in molecular systems*, Phys. Scr., 20 (1979), pp. 387–394.

[18] L. M. Degtyarev, V. G. Nakhankov, and L. I. Rudakov, *Dynamics of the formation and interaction of Langmuir solitons and strong turbulence*, Sov. Phys. JETP, 40 (1974), pp. 264–268.

[19] R. O. Dendy, *Plasma Dynamics*, Oxford University Press, Oxford, UK, 1990.

[20] B. Engquist and A. Majda, *Absorbing boundary conditions for the numerical simulation of waves*, Math. Comp., 31 (1977), pp. 629–651.

[21] L. C. Evans, *Partial Differential Equations*, AMS, Providence, RI, 1998.

[22] K. Feng, *Asymptotic radiation conditions for reduced wave equations*, J. Comput. Math., 2 (1984), pp. 130–138.

[23] W. Gautschi, *Numerical integration of ordinary differential equations based on trigonometric polynomials*, Numer. Math., 3 (1961), pp. 381–397.

[24] J. Ginibre, Y. Tsutsumi, and G. Velo, *The Cauchy problem for the Zakharov system*, J. Funct. Anal., 151 (1997), pp. 384–436.

[25] D. Givoli, *Numerical Methods for Problems in Infinite Domains*, Elsevier, Amsterdam, 1992.

[26] R. Glassey, *Convergence of an energy-preserving scheme for the Zakharov equations in one space dimension*, Math. Comp., 58 (1992), pp. 83–102.

[27] V. Grimm, *On error bounds for the Gautschi-type exponential integrator applied to oscillatory second-order differential equations*, Numer. Math., 100 (2005), pp. 71–89.

[28] V. Grimm, *A note on the Gautschi-type method for oscillatory second-order differential equations*, Numer. Math., 102 (2005), pp. 61–66.

[29] H. Hadouaj, B. A. Malomed, and G. A. Maugin, *Dynamics of a soliton in a generalized Zakharov system with dissipation*, Phys. Rev. A, 44 (1991), pp. 3925–3931.

[30] H. Hadouaj, B. A. Malomed, and G. A. Maugin, *Soliton-soliton collisions in a generalized Zakharov system*, Phys. Rev. A, 44 (1991), pp. 3932–3940.

[31] M. Hochbruck and Ch. Lubich, *A Gautschi-type method for oscillatory second-order differential equations*, Numer. Math., 83 (1999), pp. 402–426.

[32] M. Hochbruck and A. Ostermann, *Exponential integrators*, Acta Numer., 19 (2010), pp. 209–286.

[33] Y. Ji and H. Ma, *Uniform convergence of the Legendre spectral method for the Zakharov equations*, Numer. Methods Partial Differential Equations, 29 (2013), pp. 475–495.

[34] S. Jin, P. A. Markowich, and C. Zheng, *Numerical simulation of a generalized Zakharov system*, J. Comput. Phys., 201 (2004), pp. 376–395.

[35] N. Masmoudi and K. Nakanishi, *Energy convergence for singular limits of Zakharov type systems*, Invent. Math., 172 (2008), pp. 535–583.

[36] R. I. McLachlan and G. R. W. Quispel, *Splitting methods*, Acta Numer., 11 (2002), pp. 341–434.
[37] P. K. Newton, *Wave interactions in the singular Zakharov system*, J. Math. Phys., 32 (1991), pp. 431–440.
[38] T. Ozawa and Y. Tsutsumi, *The nonlinear Schrödinger limit and the initial layer of the Zakharov equations*, Proc. Japan Acad. A, 67 (1991), pp. 113–116.
[39] G. L. Payne, D. R. Nicholson, and R. M. Downie, *Numerical solution of the Zakharov equations*, J. Comput. Phys., 50 (1983), pp. 482–498.
[40] N. R. Pereira, *Collisions between Langmuir solitons*, Phys. Fluids, 20 (1977), pp. 750–755.
[41] S. H. Schochet and M. I. Weinstein, *The nonlinear Schrödinger limit of the Zakharov equations governing Langmuir turbulence*, Comm. Math. Phys., 106 (1986), pp. 569–580.
[42] L. Stenflo, *Nonlinear equations for acoustic gravity waves*, Phys. Scr., 33 (1986), pp. 156–158.
[43] C. Sulem and P. L. Sulem, *Regularity properties for the equations of Langmuir turbulence*, C. R. Acad. Sci. Paris Sér. A Math., 289 (1979), pp. 173–176.
[44] C. Sulem and P. L. Sulem, *The Nonlinear Schrödinger Equation*, Springer-Verlag, New York, 1999.
[45] B. Texier, *Derivation of the Zakharov equations*, Arch. Ration. Mech. Anal., 184 (2007), pp. 121–183.
[46] M. Thalhammer, *High-order exponential operator splitting methods for time-dependent Schrödinger equations*, SIAM J. Numer. Anal., 46 (2008), pp. 2022–2038, https://doi.org/10.1137/060674636.
[47] Y. Xia, Y. Xu, and C. Shu, *Local discontinuous Galerkin methods for the generalized Zakharov system*, J. Comput. Phys., 229 (2010), pp. 1238–1259.
[48] V. E. Zakharov, *Collapse of Langmuir waves*, Sov. Phys., 35 (1972), pp. 908–914.